Temperature Dependent Structural, Electronic and Optical Properties of the Si(100) Surface from First Principles

by

Robert Minnings

**A thesis submitted to the
School of Graduate and Postdoctoral Studies in partial
fulfillment of the requirements for the degree of**

Master of Science, in the program Modelling and Computational Science

at

The Faculty of Engineering and Applied Science,

The University of Ontario Institute of Technology,

Oshawa, Ontario, Canada

April 2019

THESIS EXAMINATION INFORMATION

Submitted by: **Robert Minnings**

Master of Science in **Modelling and Computational Science**

Thesis title: **Temperature Dependent Structural, Electronic and Optical Properties of the Si(100) Surface from First Principles**

An oral defense of this thesis took place on April 11th, 2019 in front of the following examining committee:

Examining Committee:

Chair of Examining Committee	Dr. Mehran Ebrahimi
Research Supervisor	Dr. Anatoli Chkrebtii
Research Co-supervisor	n/a
Examining Committee Member	Dr. Sean Bohun
Examining Committee Member	n/a
University Examiner	n/a
External Examiner	Dr. Franco Gaspari

The above committee determined that the thesis is acceptable in form and content and that a satisfactory knowledge of the field covered by the thesis was demonstrated by the candidate during an oral examination. A signed copy of the Certificate of Approval is available from the School of Graduate and Postdoctoral Studies.

ABSTRACT

The results presented here were obtained using the local density approximation (LDA) to density functional theory (DFT), within the pseudo-potentials scheme.

We present the results of the numerical simulations for the Si bulk and Si(100) surface; ab-initio molecular dynamics (AIMD) using the Car-Parrinello Molecular Dynamics formalism (CPMD) and Born-Oppenheimer Molecular Dynamics (BOMD), related vibrational states (surface phonons) by calculating the vibrational density of states (VDOS) using a harmonic and anharmonic approach, and the optical response of the Si bulk and Si(100) surface calculating the temperature dependent reflectance anisotropy (RA).

The surface reconstruction and temperature stimulated dimer flip impacts the surface reconstruction dynamics, the surface band gap and the optical response. For the calculated optical response and phonon spectra real temperature dependent atomic motion has been incorporated into the numerical formalism explicitly. This allows us to calculate the above materials' properties, and reach an agreement with experiment, at different temperatures.

Keywords: DFT; Si(100); Dimer; Optical Response; Temperature

AUTHOR'S DECLARATION

I hereby declare that this thesis consists of original work of which I have authored. This is a true copy of the thesis, including any required final revisions, as accepted by my examiners.

I authorize the University of Ontario Institute of Technology to lend this thesis to other institutions or individuals for the purpose of scholarly research. I further authorize University of Ontario Institute of Technology to reproduce this thesis by photocopying or by other means, in total or in part, at the request of other institutions or individuals for the purpose of scholarly research. I understand that my thesis will be made electronically available to the public.

Robert Minnings

STATEMENT OF CONTRIBUTIONS

The work described in Section 5 was performed on the computer clusters run and maintained by Sharcnet (https://www.sharcnet.ca). I was responsible for running the simulations whose results are documented in this thesis, and collecting and presenting the results. My supervisor Dr. Anatoli Chkrebtii provided assistance in determining which simulations to run and the analysis of the results of these simulations. Dr. Anatoli Chkrebtii also reviewed the thesis and provided review comments.

The relevant numerical formalisms and research results from Section 5, were presented at two conferences, namely (i) 15th International Conference on Vibrations at Surfaces (VAC15), June 22-26, 2015, Donostia-San Sebastian, Spain; (ii) International Conference on Modern Materials and Technologies (CIMTEC 2016), June 5 – 9, 2016, Perugia, Italy; and (iii) also published in Advances in Science and Technology **98**, pp. 117-124, 2017.

I hereby certify that I am the sole author of this thesis and that no part of this thesis has been published or submitted for publication. I have used standard referencing practices to acknowledge ideas, research techniques, or other materials that belong to others. Furthermore, I hereby certify that I am the sole source of the simulations and results presented in this thesis.

ACKNOWLEDGEMENTS

I would like to acknowledge the help provided by my thesis supervisor Prof. Anatoli Chkrebtii (publications under Shkrebtii) who I have worked with for several years now. I would like to especially thank him for the help in analyzing the results and for the review of the thesis. Also, a big thank you to Anatoli for all the help provided running the simulations and the physics discussions related to this.

Additionally, I would like to thank all my lecturers for the taught material for the “M.Sc. in Computational Science”.

The CPU time was provided by the Shared Hierarchical Academic Research Computing Network (Sharcnet) of Ontario, Canada.

Finally, I would thank UOIT for providing a part time option for this Master’s Course.

Contents

LIST OF FIGURES and TABLES

LIST OF ACRONYMS

Acronym	Description
(xxx), i.e., (100)	Indicates a specific surface (i.e., surface plane)
[xxx], i.e., [110]	Indicates a direction, perpendicular to [xxx] surface
AIMD	Ab Initio Molecular Dynamics
BO	Born Oppenheimer approximation, used to solve the Schrodinger Equation
BOMD	Born-Oppenheimer Molecular Dynamics
CPMD	Car-Parrinello Molecular Dynamics
c(2×4)	A specific surface configuration of surface dimers called reconstruction
DB	Dangling Bond
DFT	Density Functional Theory
DFPT	Density Functional Perturbation Theory
DOS	Density Of States
EELS	Electron Energy Loss Spectroscopy
FCC	Face Centered Cubic
HEG	Homogenous Electron Gas
HREEL	High Resolution Electron Energy Loss
LDA	Local Density Approximation
LEED	Low Energy Electron Diffraction
MD	Molecular Dynamics
p(2×1)	A specific surface configuration of surface dimers, 2×1 reconstruction
p(2×2)	A specific surface configuration of surface dimers, 2×2 reconstruction
QE	Quantum Espresso. The software package used in this thesis
RA	Reflectance Anisotropy
RAS	Reflectance Anisotropy Spectroscopy
Si(xxx), i.e. Si(100)	Indicates a surface of Si, i.e., a plane
STM	Scanning Tunneling Microscopy
VDOS	Vibrational Density of States. (i.e., phonon states)

1 Introduction

Silicon is a cornerstone of the modern electronics industry, and its two low index reconstructed surfaces Si(100) and Si(111) are among the most important and well characterized systems. The clean Si(110) surface that has a very complex reconstruction, in contrast, is still not well understood. Low index clean Si surface reconstructions consist of a variety of the typical building blocks, such as dimer, adatom, missing atom, 1D-chains, *etc*., [2]. Since Si(100) is the main surface of the electronics Industry, we will model here this technologically significant Si(100) surface and its dimer based reconstructions.

Additionally, Si(100) is the substrate for creation of the Si – Ge strained superlattices, that have already found numerical applications in microelectronics, such as electrically pumped lasers from the Germanium-on-Silicon *pnn* hetero-junction diode [3]. Optical and vibrational spectroscopies are very important tools in understanding the surface systems [4], [5].

Furthermore, creating silicon and silicon compounds as wafers, a key requirement for the electronics industry, uses a process called epitaxy. The Si (100) surface and its structure has a critical impact on the efficacy of the different forms of epitaxy when Si (100) is used as the substrate in this process. Therefore, an understanding of the Si (100) surface is of high importance to the modern electronics industry. Examples of this interest in Si (100) and epitaxy are [59], [60].

The main building block of all the Si(100) reconstructions is the asymmetric (or tilted) dimer, with the dimer bonds along the $[0\bar{1}1]$ direction [6--9]. The main experimentally observed clean Si(100) surface reconstructions can be created by different arrangements of tilted dimers, with examples shown in *Figure [1]* (b), (c). Although for a decade before 1990 most of the experimental and theoretical results were in favor of tilted dimers, [8], the convincing proof for asymmetric dimerization was offered later in [10--13]. The clean Si(100) reconstructed surface shows a 2 × 1 Low Energy Electron Diffraction (LEED) pattern at room temperature [8] and such a 2 × 1 reconstruction, originating from periodically repeated asymmetric dimers, can be used to fit the LEED intensity in terms of the microscopic atomic structure [14]. Regarding the microscopic details of the dimer arrangements, however, it is currently well-established that the dimers are not only tilted, but their tilt is ordered in an alternating manner along the [011] direction, thus forming c(4 × 2) and/or p(2 × 2) reconstructions of Si(100), as shown in *Figure [1],* (b), (c). These higher order reconstruction can be observed below 200K at the defect free regions of Si(100) [6,8--10,15,16]. The temperature dependent dynamical effect above 200K [10,16] or electric field of the Scanning Tunneling Microscopy (STM) tip [17,18] are responsible for the dimer flipping (flipping of the dimer tilt to the opposite orientation), and leads to apparent 2 × 1

LEED or STM patterns. The microscopic picture is that nonzero temperature dynamical affects cause the well-known structural uncertainty, namely a c(4 × 2) ↔ p(2 × 2) transition at the Si(100) reconstructed surface due to dimer flipping. The time-averaged structure is seen as an apparent 2 × 1 reconstruction. The potential barrier for dimer flipping (within 0.03 ÷ 0.11 eV [15]), leading to the c(4 × 2) and p(2 × 2) structures switching, becomes comparable with the thermal excitation energy above 200K. Such dimer dynamics is responsible for the apparent 2 × 1 LEED pattern [8,9] or STM image [16,19], [20]. Indeed, an X-ray diffraction experiment [21] has proven that Si(100) 2 × 1 structure is likely to be a disordered combination of a higher-order reconstruction, p(2 × 2) or c(4 × 2). However, the dimer flipping has also been observed below 40 K and this effect has been attributed to the Si(100)–STM-tip interaction [22,23]. Indirect proof of the higher order Si(100) reconstruction has been offered in [24]. Comparing calculated HREEL and RAS responses of the main Si(100) structures, a good agreement with the various available experimental results for the electron energy loss spectroscopy (EELS) and reflectance anisotropy spectra for c(4 × 2) structure has been obtained. Also, the calculations ruled out the presence of the p(2 × 1) reconstruction.

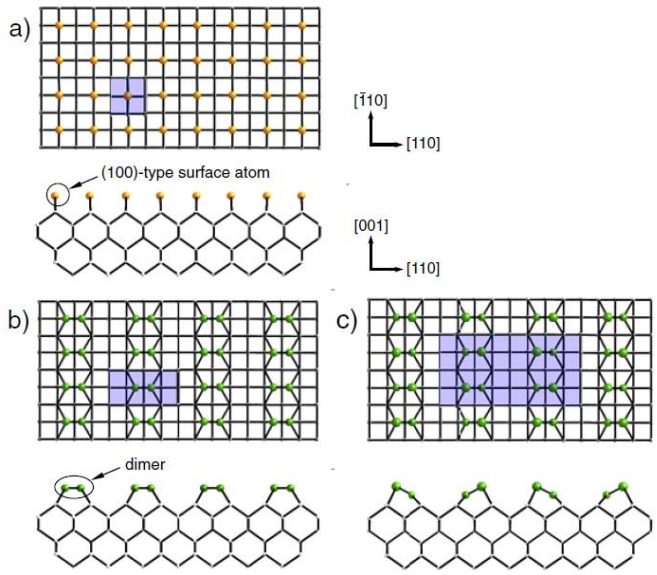

Figure 1. Clean Si(100) surface reconstruction.

a) Bulk-truncated Si(100) (1×1) surface. b) Si(100) (2×1) with symmetric dimers. (c) Si(100) (4×2) with asymmetric dimers. The corresponding unit cells are also shown highlighted in purple.

Figure 1 depicts the top and side views of the first six atomic layers of (a) the ideal bulk terminated unreconstructed p(1×1) clean Si(100) surface and dimer reconstructed clean Si(100) surfaces: (b) symmetric p(2×1) dimer and (c) asymmetric c(4×2) reconstructions. The primitive unit cells for each superstructure are illustrated by the purple shading.

Vibrational and optical spectroscopy combined with theoretical modeling are the tools of choice to accurately and non-invasively characterise various surface processes *in-situ*. Because Si(100) is one of the most fundamentally and technologically important semiconductor surfaces, its microscopic understanding is needed to enhance microelectronics device performance. A connection between dynamics and c(4×2) / p(2×2) reconstructions of the clean Si(100) surface at room temperature conditions, with an apparent (2×1) phase was established two decades ago through molecular dynamics (MD) simulations [10]. Surface vibrational spectra have also been calculated [10], [25] and confirmed experimentally (see [26] and refs. therein). However, due to dimer flipping at Si(100), the dynamical processes at the surface are highly an-harmonic. This phenomenon has not sufficiently been addressed theoretically. In addition to being responsible for a c(4×2) → (2×1) order-disorder transition near room temperature, the anharmonicity of surface vibrations substantially influences high temperature behaviour of Si(100) [4-5]. Temperature induced modification of the Si(100) optical response [10] clearly indicates the strong contribution of the dimer vibrational anharmonicity to atomic structure, electron bands and optical transitions between them.

Here we combine the molecular dynamics, numerical phonon and optical formalisms to calculate temperature-dependent vibrational spectra of the clean Si(100) surface, and then calculate the surface temperature dependent reflectance anisotropy (RA) spectra. When modeling surface vibrations, two different first principles techniques are used: (i) highly accurate density-functional perturbation theory (DFPT) [27] that, however, is inherently harmonic; and (ii) postprocessing of temperature dependent MD trajectories through the Fourier transform of the velocity discrete correlation function. The second method includes anharmonicity implicitly, which is evident from our calculated spectra. To extract the vibrational density of states (VDOS), finite temperature Car-Parrinello Molecular Dynamics (CPMD) runs were carried out at temperatures of 300K and 600K to provide temperature-dependent atomic structural input. When calculating the optical response at nonzero temperature, the vibrational anharmonicity was included through averaging the calculated optical response for several representative temperature-perturbed atomic configurations (snapshots). Agreement with experimental results [56] is demonstrated, including a temperature-induced shift of both surface and bulk optical peak to lower energy and broadening, while the temperature-induced effects are shown as more pronounced for the surface atoms than for the Si bulk atoms.

An important difference, compared to current results from the published literature, for the calculated optical response and phonon spectra, is that for the first time, real temperature dependent atomic motion has been incorporated into the numerical formalism explicitly. This allows us to actually calculate the above materials' properties and reach an agreement with the experiment [56], at different temperatures.

2 Main Physics Concepts and Theory as they apply to this Thesis

We first (Section 2.1) discuss the topic of surface reconstruction, which is pertinent to the results and discussion in this thesis, for the Si(100) surface. A phenomenon known as dimer flipping, which we observe theoretically is also discussed.

The mathematical model and approximations used to simulate Molecular Dynamics and obtain Density of States and the Linear Optical Response is then discussed (Section 2.2).

2.1 *Surface Reconstruction*

The atomically clean surface of a semiconductor, in this case Si(100), will have a different atomic geometry than the atoms in the bulk (the non-surface atoms), or for the bulk–like ideally terminated surface. It is unstable due to the presence of the unsaturated covalent bonds, created when the clean surface is formed.

At the surface, which is created by cutting or cleaving of the covalent bonds, the interatomic forces on the nuclei, associated with the top atoms and atoms underneath the surface, are not balanced anymore by equal and opposite forces on the surface side.

The result is that the atoms at or near the surface are not in equilibrium. There will then be movement of these top atoms into new positions to saturate the so- called dangling bonds (DBs), which minimizes the total energy and form the new equilibrium structure. The result of this rearrangement is referred to as surface reconstruction or relaxation. For the relaxed surfaces the symmetry of the bulk-terminated surface is preserved, therefore they are always called (1×1) relaxed structures. For the surface relaxation, however, the new surface periodicity is different to that of the bulk terminated structures [9].

Several theoretical techniques have been developed over the recent few decades [28]. Among them, Density Functional Theory (DFT) [29] can be used to accurately simulate Si(100) surface structure, surface states and vibrations as it makes no assumption about the equilibrium configuration. The solution of the full Quantum Mechanical Equation (subject to certain approximations) can be used to determine the equilibrium structure of the surface.

To simulate the clean Si(100) surface, we use an artificial 3d periodic system, within the so-called repeated slab geometry. One Si(100) slab consists of 64 Si atoms arranged in 8 layers. The bottom two Si(100) layers have H atoms (16 in total) to saturate dangling Si bonds from the bottom surface. The lower Si atoms and H atoms (last two Si layers and H layer) are kept stationary in the

model to simulate a crystal that is very thick, that is the forces at the surface have no impact on the lower atoms. As the first step of the numerical simulations, the equilibrium atomic structure of the surface can be determined by performing DFT based optimization – (see Sec 6.2 for the formalisms used). Starting with the ideal surface p(1×1), the atoms at the surface are connected with only two bonds to the neighbor below (in contrast to the bulk bond arrangement), and are effectively directed upright. Clearly, this is an unstable configuration and has the highest energy.

To reduce the energy of the ideally terminated surface, the main structural changes are due to dimerization: the top Si(100) atoms, belonging to parallel rows form new bonds with each other, called dimers. This pulls the atoms down from adjacent rows into either a symmetric p(2 × 1) or asymmetric p(2 × 1) pattern. *Figure 2* demonstrates the transition from the unrelaxed Si(100) 1×1 structure to Si(100) symmetric p(2 × 1).

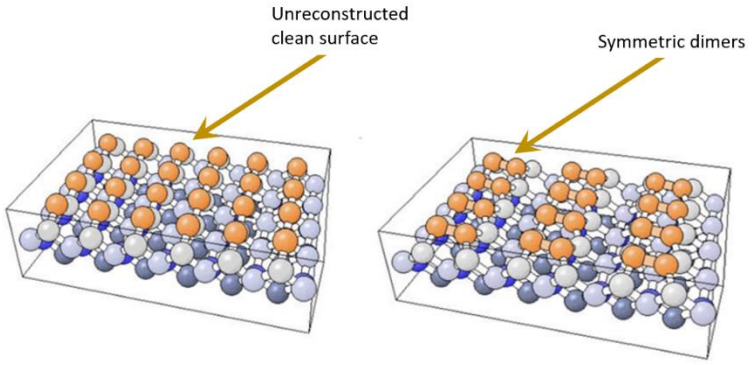

Figure 2. Clean Si(100) unreconstructed (left), and (2×1) reconstructed with symmetric dimers Si(100) surface (right), perspective view. (The different colors represent atoms in different layers)

<u>Left:</u> Unreconstructed Si(100) (1×1) surface. The Si atoms of the topmost layer are highlighted in orange. These atoms are bonded to only two other Si atoms, both of which are in the second layer (shaded grey).

<u>Right:</u> Reconstructed Si(100) (2×1) surface. The Si atoms of the topmost layer form a covalent bond with an adjacent surface atom and are drawn together as pairs. They are said to form dimers, which are symmetric.

The change from the ideal Si(100) p(1×1) to the symmetric dimer pattern p(2×1) reduces the total energy of the surface, giving an energy gain of approximately 0.2 eV per dimer [30].

The formation of dimers can be explained as follows, see *Figure 3*. The Si atom has four valence electrons. For the surface atom, two of these atoms form bonds with the atom immediately below. The remaining two electrons form two surface dangling bonds. This results in four half-filled orbitals for every pair of Si atoms.

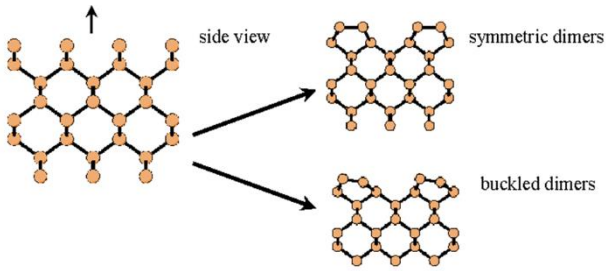

Figure 3.Clean Si(100) surface symmetric and buckled dimers for the p(2×1) reconstruction. The dimers are seen at the top of the two pictures to the right. When parallel to the X-Y plane (plane coming out of paper) they are called symmetric, and when at an angle to the X-Y plane, they are called buckled or asymmetric dimers.

This ideal bulk terminated structure is highly unstable and has no gap (that is metallic) due to unpaired electrons. To reduce the total energy the system rearranges to have three orbitals occupied, two dangling ones and a third one in between the two atoms of the dimer forming the main structure unit of the clean Si(100) surface. The dangling bonds will be singly occupied while the dimer bond will be doubly occupied. That is, the symmetric dimers still demonstrate the absence of the surface band gap. Relative to the ideal surface structure this configuration has a lower energy by approximately 2 eV per dimer. [30].

The energy can be reduced further by tilting the dimer bonds, see *Figure 3*. This reduces the energy by approximately 0.2 eV per dimer. Important to note, is that the tilting of the dimer opens the surface band gap [9], thus making the Si(100) surface semiconducting. This effect, predicted theoretically, has been observed experimentally.

The energy can be reduced yet further (close to 0.02 eV per dimer) by alternating the tilt angle from dimer row to row, see *Figure 4*, resulting in the p(2×2) reconstruction. Further, by having adjacent dimer rows which are mirror images of each other, a c(4×2) configuration results. The energy difference between these two configurations is than numerical accuracy and the energy

difference between the p(2×1) and the p(2×2) or c(4×2) configurations. Even though and this energy difference has not been directly confirmed experimentally, STM measurements indicate that p(2×2) and c(4×2) are practically degenerate in energy.

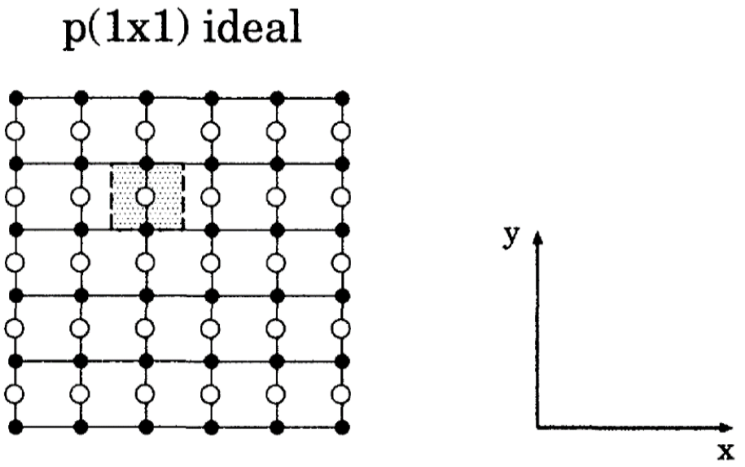

Figure 4a

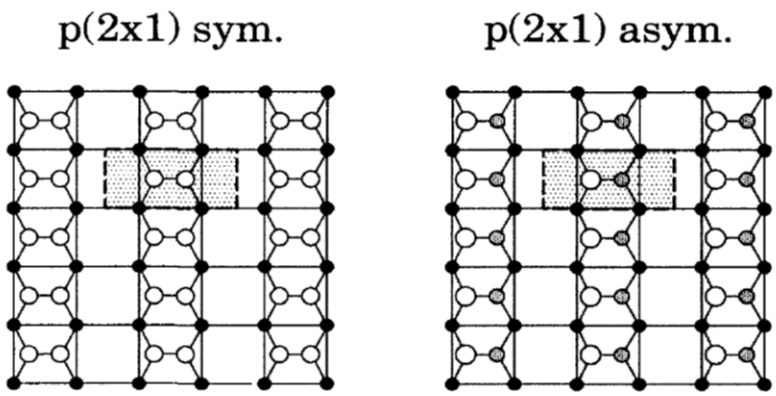

Figure 4b

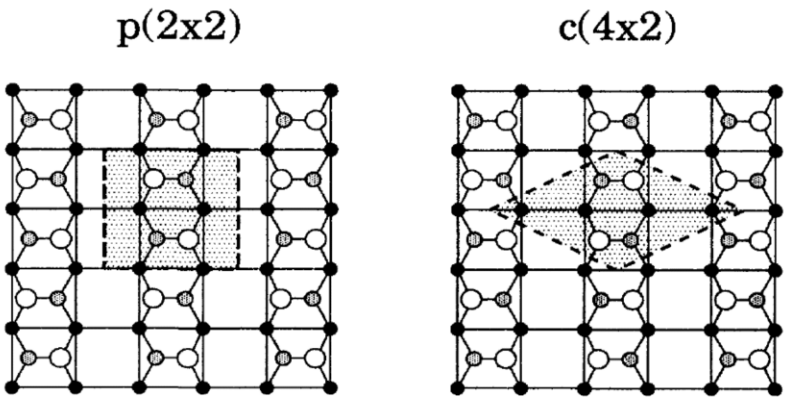

Figure 4c

Note: In the images above, the grey depicts atoms lower than the white atoms. The grey shading indicates the primitive unit cell. Note that the higher(white) atoms relative positions on the right diagram c(4×2) are different to the higher atoms relative positions on the diagram on the left p(2×2). This is clearly shown in the diagram below, 4d.

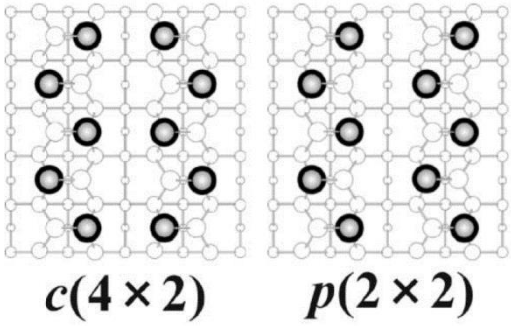

Figure 4d

Note: Difference between c(4×2) and p(2×2) looking from the top of the surface.

Figure 4. Si(100) surface reconstruction nomenclature. Starting with the ideal bulk-terminated (100) surface (Figure 4a), then it shows the p(2×1) symmetric and asymmetric reconstructions (Figure 4b), and then Figures 4c and 4d show the higher-order p(2×2) and c(4×2) reconstructions.

Figure 5 depicts the calculated energy differences between the ideal bulk-terminated Si(100) (1×1) surface and different reconstructions. It shows the p(1×1) ideal structure with the highest energy (meaning that this structure is unstable), and the p(2×1) symmetric structure with an energy difference of 2eV per dimer from the p(1×1) ideal structure. The other reconstructions, namely c(4x2) and p(2x2), are shown with their corresponding energy differences per dimer.

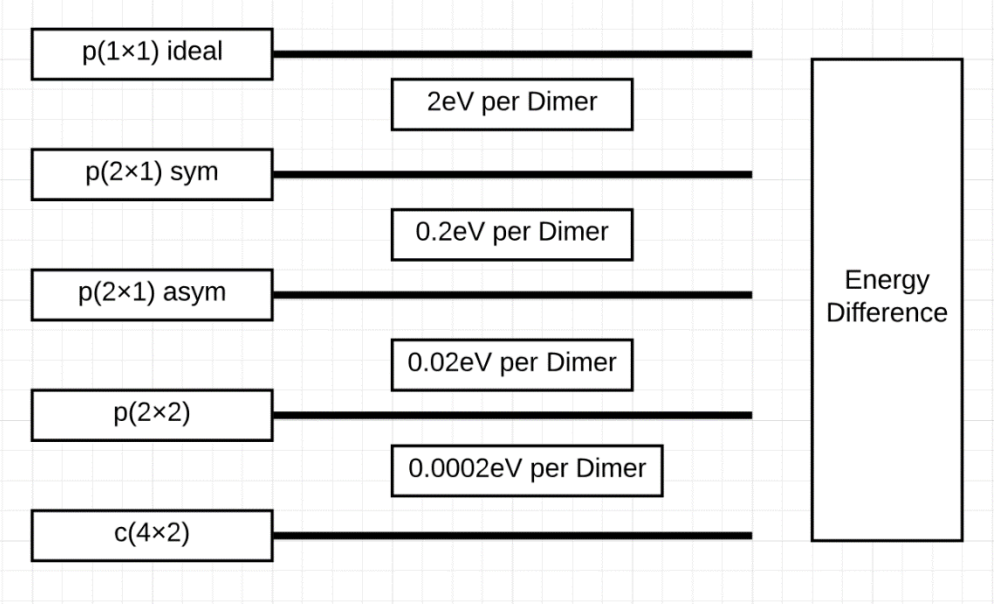

Figure 5. Calculated total energy differences (per dimer) for the main reconstructions at the clean Si(100) surface (from [30]), starting with the ideal bulk truncated Si(100). This shows that the most stable (lowest energy) and therefore most likely occurring surface configurations are p(2×2) and c(4×2).

The total energy difference makes it clear that the dimers at the low temperature should be buckled rather than symmetric. Furthermore, the p(2x1) Si(100) reconstruction should be unstable with respect to formation of the higher order p(2×2) and c(4×2) reconstructions, this leads to alternating dimer tilts within the same row. Given the small energy difference between the p(2×2) and p(4×2) configurations, local temperature dependent fluctuations may lead to surface domains with different higher order reconstructions.

It is also possible for a higher order reconstruction to transform to another over a time period. The p(2×1) asymmetric, and p(2×2), c(4×2) have been observed at the same surface location at different times. This phenomenon is due to dimer flipping as described below.

Two dimer states, based upon the dimer tilt angle, ("up" – $(+\alpha)$/ "down" – $(-\alpha)$), can be represented by a double potential well, see *Figure 6.*

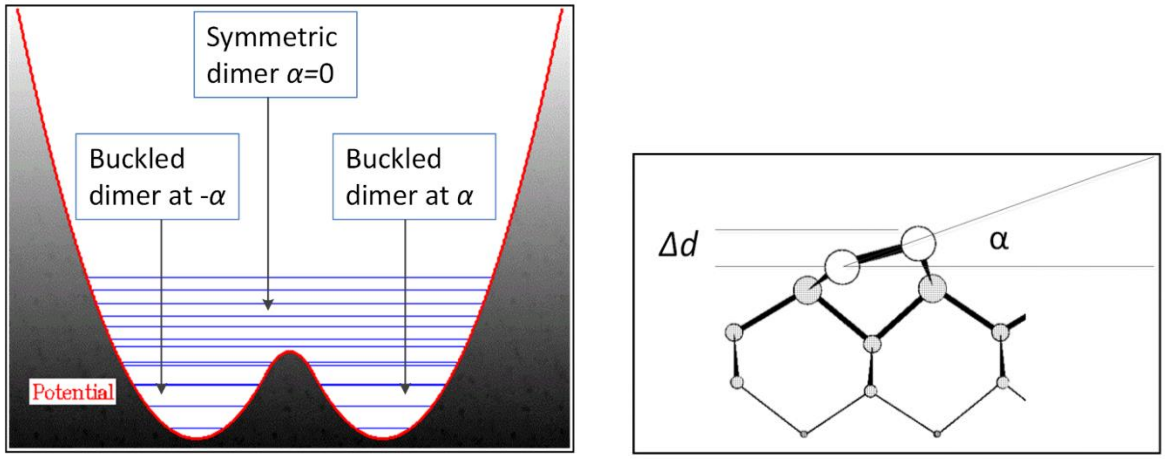

Figure 6. Double potential well and dimer tilt angle for Si(100) surface.

<u>Left:</u> Red line indicates tilting angle dependent potential energy of the dimer. Blue lines indicate allowed potential energy levels of the dimer. Graphic illustrates that a symmetric dimer has a higher potential energy than an asymmetric (buckled) dimer

<u>Right:</u> Large white circles represent the two atoms in the dimer. Graphic illustrates the dimer angle α to the surface plane and the relative height Δd of the second dimer atom relative to the first

Figure 6 illustrates the quantum vibrational Levels (horizontal lines) for a dimer. At temperatures where the thermal energy $kT \sim \Delta E$, the dimer state can flip to a new energy level and hence a new configuration. The term dimer flipping is used to describe this occurrence, and we show later that dimer flipping occurs in the molecular dynamic runs at a temperature of approximately 600 K. A dynamic mixture of c(4x2) and p(2x2), due to dimer flipping can be observed during molecular dynamic runs at this temperature.

Experimentally dimer flipping has been observed at room temperature [19,20], starting at 200K, however the probability of a dimer flip increases with increasing temperature due to the higher kinetic energy, associated with the temperature increase. In such a case, a higher temperature makes it more probable for the dimers to overcome the potential energy barrier. As the molecular dynamic runs are necessarily (due to computational power limitations) completed over a very short real time (order of femto-seconds), the probability of a dimer flip at simulated room temperature is much less than at the higher temperature and the fact it is not observed computationally with runs of this time length. In our several week-long simulations at 300K we did not actually see dimer flipping. At 600K we observed several flipping events, as discussed below. It is possible to extend the number of Quantum Espresso MD steps at this temperature

and to run for months in order to try to obtain this result. Longer MD runs for this case can be suggested for future work.

2.2 *Mathematical Model and Numerical Formalism*

The mathematical model and approximations in Molecular Dynamics simulation to obtain the macroscopic atomic structure, electrons band gap, electron and vibrational density of states (DOS and VDOS) and the Linear Optical Response are discussed in this section and its sub-sections. The primary theory behind the numerical simulation is referred to as Density Functional Theory (DFT).

We will not go into the details of Density Functional Theory (DFT) formalism in this thesis. However, it would be pertinent to list some examples used in the formalism in conjunction with DFT in order to carry out the numerical simulations. Detailed descriptions of DFT can be found in many monographs or reviews, see for instance, [29].

In this section we list various techniques and approximations used in order to computationally solve the many body Schrodinger Equation for the confined systems, such as surfaces, which is the starting point for Ab-Initio (or first principles) molecular dynamics simulations.

In order to simulate the properties and atomic motion of the Si crystals of interest we start with the many-body Schrodinger Equation, including several contributions to the many-body potential. Equation (1) is the time independent many-body Schrodinger Wave Equation, used to calculate the complex wave functions $\psi(r_1, r_2, \dots)$:

$$\left(-\sum_i \frac{\nabla_i^2}{2} - \sum_I \frac{\nabla_i^2}{2M_I} - \sum_{i,I} \frac{Z_i}{|r_i - R_I|} + \frac{1}{2}\sum_{i \neq j} \frac{1}{|r_i - r_j|} + \frac{1}{2}\sum_{I \neq J} \frac{Z_I Z_J}{|R_I - R_J|}\right)\psi = E_{tot}\psi, \quad (1)$$

where the units are Hartree atomic units (electron mass is the unit of mass and the electron charge is set to e = 1), and M_I is the mass of the nuclei, R_I is the nuclei position, r_i the electron positions, Z_I the nuclei atomic numbers. Starting with the terms from the left hand side of the equation, the first term is the electron kinetic energy, the second term is the nuclear kinetic energy, the third term is the electronic-nuclear attraction, the fourth term describes the electron-electron repulsion and lastly the fifth term is the nuclear-nuclear repulsion.

This equation includes all information about a material in equilibrium without any external perturbations such as, e.g., electromagnetic wave, external magnetics or electric fields, *etc*.

(Note: In Equation (1) the corrections due to relativity can be applied for “fast moving electrons”, that is heavy elements, but for the purposes of the simulations in this thesis these corrections

are not important: Si atoms demonstrate negligible spin-orbital interaction and do not have significant impact on the results).

The solution of this equation gives the ground state energy (eigenstate with the lowest electronic energy) of the system (material) under consideration and its many body wave function. With this microscopic ground state energy and the wave function, many equilibrium macroscopic properties of materials can be calculated. However, the order of the equation increases exponentially with the size of the system and therefore in the form above it is not solvable apart from very small systems. Therefore, several approximations, described below, need to be used to numerically solve equation (1).

We describe the main approximations used in the sub-sections below. We also provide a summary table 1 below of these approximations and techniques to aid the reader.

Technique/Approximation	**Brief Description**
Clamped Nuclei Approximation	Set the Nuclei mass to infinite (temporarily). Results in Nuclei attraction and repulsion terms in (1) going to constant values. This is necessary for the electron ground state minimization.
Born-Oppenheimer Approximation	Use classical dynamics to calculate the motion of the nuclei. The requirement for the cores to be fixed (clamped nuclei) is now removed. It allows us to decouple electron and ion subsystems. The force on the nuclei are calculated using Quantum Mechanics.
Independent Electrons Approximation	Assume that there is "no repulsion between electrons" though the one-electron approximation This results in N three dimensional equations in place of the 3N dimensional coupled equation (i.e., separating (1) into multiple equations).
Mean Field Approximation	Every electron experiences an average potential (mean field) due to the other electrons. The average potential is calculated via the Poisson Equation through a self-consistent numerical computation.
Hartree-Fock Approximations	The Fock exchange potential $V_X(\boldsymbol{r}, \boldsymbol{r}')$ term, derived using Quantum Mechanics, is added to the Mean Field Approximation.
Kohn-Sham Equations	Add the Exchange and Correlation Potential $V_{xc}(\boldsymbol{r})$ in efficient and easy treated term. (This term now includes the Fock exchange potential.) This leads to E_{xc}, the exchange and correlation energy, required in order to accurately model the material ground state.

LDA Approximation	An approximation to substitute nonlocal exchange-correlation potential E_{xc}. Uses data from a Homogenous Electron Gas, and sums over local electron densities in the material being modelled.
Plane Wave Expansion	Uses Fourier series to expand the solution waveforms.
k-Point Sampling	Methods to select a finite number of wave vectors (***k***-points), for the Fourier series expansion of the solution waveforms.
Pseudo Potential	Replace the core electrons of the material with a pseudo potential. This saves on computation cycles.
Self-Consistent Calculations	A method to solve equations where you have dependent unknown variables.
Hellman-Feynman Theorem	The Hellman-Feynman theory states that we can obtain forces F_I for all nuclear coordinates by using the electron density *n(**r**)* for ONE set of nuclear coordinates only.

Table 1. Summary of main approximations used in the model described in the following sub sections.

2.2.1 The Clamped Nuclei Approximation

In solids at equilibrium and especially crystals the nuclei do not move very far from their equilibrium positions. An approximation can be used, temporarily setting the nuclei mass to infinite in *Equation (1)*, and therefore the corresponding nuclear coordinates can be considered as fixed (in a separate step of the numerical formalism, the nuclei are moved according to the laws of classical mechanics). This approximation results in the kinetic energy term for the nuclei going to zero, and the nuclei Coulomb potential becomes a constant, and therefore temporarily removes the two terms,

$$\sum_{i,I} \frac{Z_i}{|r_i - R_I|}, \quad \frac{1}{2} \sum_{I \neq J} \left(\frac{Z_I Z_J}{|R_I - R_J|} \right)$$

that deal with nuclei attraction and repulsion as variables from *Equation (1)*. The remaining equation is then the fundamental equation of electronic structure theory and resembles the single particle Schrodinger equation, but with multiple electrons and their mutual Coulomb repulsion.

2.2.2 The Born-Oppenheimer Approximation

The clamped nuclei approximation described in the section above, is used in one stage of the numerical formalism. However, in order to model a solid accurately using the Car-Parrinello or Born Oppenheimer approaches for molecular dynamics used in this thesis, the nuclei vibration (movement) has to be considered. A technique to model the nuclei motion, is to use classical mechanics applied to the nuclei (i.e., force applied to the nuclei results in classical motion). However, the forces on the nuclei are calculated by using Quantum Mechanics whilst the nuclei are fixed in position. Classical dynamics with the calculated force on the nuclei as the input, is then used at each time step of the molecular dynamics simulation. This use of classical dynamics for the nuclei is known as the Born-Oppenheimer approximation. In effect as will be described later, the approximation gives two decoupled Schrodinger equations, one for the electrons and one for the nuclei.

2.2.3 The Independent Electrons Approximation

The term in *Equation (1)* describing the Coulomb repulsion between electrons,

$$\frac{1}{2} \sum_{i \neq j} \frac{1}{|r_i - r_j|}$$

can be removed from consideration if we assume that the electrons do not “see” each other (i.e., no Coulomb force felt from the other electrons).

The solution to the Schrodinger Equation, *Equation (1),* for the many electrons now implies that the probability of finding an electron 1 at position r_1 and electron 2 at r_2 is given by the product of the individual probabilities of finding the electrons at those positions, i.e., the Schrodinger Equation can be decomposed into the product of the probability function of each electron.

Defining the single electron Hamiltonian as

$$\widehat{H}_0(\boldsymbol{r}) = -\frac{1}{2}\nabla^2 + V_n(\boldsymbol{r}), \qquad (2)$$

then the multi body Schrodinger equation within the independent electrons approximation is

$$\sum_i \widehat{H}_0(\boldsymbol{r_i})\,\Psi = E\,\Psi. \qquad (3)$$

As the electrons are independent, the solution to (3), $\Psi(\boldsymbol{r_1}, \ldots\ldots \boldsymbol{r_n})$, can be given as the product of the probability of each electron as a function of position, i.e. the product of the single electron wavefunctions,

$$\Psi(\boldsymbol{r_1}, \ldots \boldsymbol{r_n}) = \phi_1(\boldsymbol{r_1}) \ldots \times \ldots \phi_n(\boldsymbol{r_n}). \qquad (4)$$

Here the interchange $r_i \leftrightarrow r_j$ is still possible. The Pauli exclusion principle, which does not allow this interchange, will be included later. This then gives for (3), in the form:

$$[\sum_i \widehat{H}_0(\boldsymbol{r_i})]\,\phi_1(\boldsymbol{r_1}) \ldots\ldots\ldots \phi_n(\boldsymbol{r_n}) = E\,\phi_1(\boldsymbol{r_1}) \ldots\ldots\ldots \phi_n(\boldsymbol{r_n}). \qquad (5)$$

And for each electron, given that the ϕ_I are independent, we can write:

$$\widehat{H}_0(\boldsymbol{r})\phi_I(\boldsymbol{r}) = \varepsilon_i\phi_I(\boldsymbol{r}). \qquad (6)$$

Here the energy *E* from (5) is given by $E = \varepsilon_1 + \cdots \ldots \varepsilon_n$, and ε_1 is the smallest eigenvalue for the single electron solution (6), ε_2 the next smallest etc.

This product form for the solution (5), provides a mechanism for the numerical solution of the Schrodinger equation. The *3N* dimensional many-body Schrodinger wave equation is now replaced by *N* three dimensional equations.

However, the magnitude of the Coulomb repulsion between electrons term is comparable to the magnitude of the other terms so it cannot just be ignored. This necessitates the addition of other terms into the equation to account for this force, see the immediate sections below.

2.2.4 Mean Field Approximation

As mentioned in the previous section the electron – electron repulsion cannot be ignored. As one approximation, an average potential experienced by every electron can be derived.

Using Poisson's equation and the electron charge distribution, the concept of an average potential (mean field) experienced by every electron can be derived.

Assuming independent electrons as discussed above, the electron charge density ***n(r)*** can be obtained by adding up the individual probabilities of finding electrons in each occupied state

$$n(\mathbf{r}) = \sum_i |\phi_i(r)|^2. \qquad (7)$$

Using classical electrostatics, the potential due to this charge density, called the Hartree potential, is

$$\nabla^2 V_H(r) = -4\pi n(\mathbf{r}). \qquad (8)$$

Equation (6) can now be modified by adding V_H as below:

$$[\,\widehat{H}_0(\boldsymbol{r}) + V_H(\boldsymbol{r})]\phi_i\,(\boldsymbol{r}) = \varepsilon_i\phi_I\,(\boldsymbol{r}), \qquad (9)$$

as $V_H(\boldsymbol{r})$ is experienced by all the electrons and is an average potential, hence defining the term Mean Field Approximation (see, e.g., [28]).

Equations (7), (8), (9) must be solved simultaneously. At each step of the simulation the $V_H(\boldsymbol{r})$ from (8), calculated from $\phi_i(r)$ used in (7), must return $\phi_i(r)$ in (9). This method is called a self-consistent field method [28].

However, this approximation is not accurate enough for atomistic scale modelling and to improve the simulation two more contributions, namely exchange potential and correlation potential are required. This can be included through the Hartree-Fock formalism described in the next section.

2.2.5 Hartree – Fock Approximations

To improve the accuracy of the electron-electron repulsion calculation another term must be added to *Equation (9)*.

Assume that the electrons do interact, but the interaction is not too strong. The single particle wave functions $\phi_i(\mathbf{r})$, used in the independent electrons approximation can be calculated using a variation principle. [29]

As previously discussed, the wave function in the Hartree approximation can be described as:

$$\Psi\,(\boldsymbol{r_1}, \ldots\ldots \boldsymbol{r_n}) = \phi_1\,(\boldsymbol{r_1}) \ldots\ldots\ldots \phi_n\,(\boldsymbol{r_n}). \qquad (10)$$

The accuracy of the wave-function (10) is not sufficient. For instance, this allows two electrons to have the identical wavefunction that is symmetric, which is incorrect for fermions. The Hartree-Fock method is to look for solutions where $\Psi\,(\boldsymbol{r_1}, \ldots\ldots \boldsymbol{r_n})$ is in the form of a Slater determinant, which makes the electron wave function asymmetric.

For instance, for a two electron system, the Slater determinant is shown below:

$$\Psi\,(\boldsymbol{r_1}, \boldsymbol{r_2}\,) = \frac{1}{\sqrt{2}}\begin{bmatrix}\phi_1\,(\boldsymbol{r_1}) & \phi_1\,(\boldsymbol{r_2})\\ \phi_2\,(\boldsymbol{r_1}) & \phi_2\,(\boldsymbol{r_2})\end{bmatrix}. \qquad (11)$$

The energy of the system is the given by

$$E = <\Psi|H|\Psi>. \qquad (12)$$

Considering the state Ψ with the lowest energy and minimizing *E* with respect to the variations of $\phi_i(\mathbf{r})$, it can be shown that a new set of equations (same as the equations in the mean field approximation but with an extra term in the Schrodinger equation) can be derived with a new term called the Fock exchange potential. This potential arises due to the fact that no two electrons can occupy the same quantum state (the Slater determinant enforces this rule), and the one-electron wave functions $\phi_i(\mathbf{r})$ are orthonormal (a condition required to normalize the probability of the wave function).

The Fock exchange potential $V_X(\boldsymbol{r}, \boldsymbol{r}')$ is another term that is now added to (9). The variables $\boldsymbol{r}, \boldsymbol{r}'$ refer to the position variable of each single electron wave function and the potential is a sum over all the occupied single particle states (i.e., interactions between all pairs of electrons)**.** The extra variable $\boldsymbol{r}'$ complicates the numerical solution and a simplified potential $V_X(\boldsymbol{r})$ is used (See Local Density Approximation (LDA) 2.2.7).

Equation (9)now becomes, with the additional term,

$$[\widehat{H}_0(\boldsymbol{r}) + V_H(\boldsymbol{r}) + V_X(\boldsymbol{r})]\phi_i\,(\boldsymbol{r}) = \varepsilon_i\phi_I\,(\boldsymbol{r}). \qquad (13)$$

It is important to note that whilst $V_H(\boldsymbol{r})$ is derived from a classical approach, $V_X(\boldsymbol{r})$ is a quantum mechanics derived approximation, mostly used in quantum chemistry. However, due to the complexity of the approach, especially when dealing with the Slater determinant, this approach is not used very often in solid state physics.

2.2.6 Kohn-Sham Equations

A further interaction between electrons needs to be incorporated into the simulation, namely, the correlation between electrons. Due to electrostatic repulsion, the probability of finding an electron near another electron must be a function of the electron-electron repulsion to some extent.

The separation of the wave equation to a product of the individual electron wave equations does not take this repulsion into account. However, the separation product is a key part of the simplification and so is left. Another term called the correlation potential is added to the equation to account for the electron-electron correlation.

The exchange correlation and a simplified Hartree Fock potential discussed in the previous section, lead to the Kohn-Sham equations which are the foundation of first principles (ab initio) materials modelling [31], [32].

In describing the ab-initio approach, we start with the total energy *E*, of the many electron system in the form:

$$E = <\psi|\widehat{H}\ |\psi> = \int d\boldsymbol{r}_1 \dots d\boldsymbol{r}_n \psi^* (\boldsymbol{r}_{1\dots\dots}\boldsymbol{r}_n)\ \widehat{H}\psi(\boldsymbol{r}_{1\dots\dots}r_n). \quad (14)$$

The Hamiltonian $\widehat{H}$, is given below, where the second term encapsulates all the electron-electron interactions.

$$\widehat{H}(\boldsymbol{r_1}, \boldsymbol{r_2} \dots\dots \boldsymbol{r_n}) = \sum_i \frac{\nabla_i^2}{2} + \frac{1}{2} \sum_{i \neq j} \frac{1}{|\boldsymbol{r_i} - \boldsymbol{r_j}|} + \sum_i V_n(\boldsymbol{r_i}). \quad (15)$$

The core concept of Density Functional Theory is that if *E* is the lowest possible energy of the system, the energy of the ground state, then *E* is a functional of the electron density only:

$$E = F(\boldsymbol{n}). \quad (16)$$

The energy of any quantum state is a functional of the entire wavefunction $\psi(\boldsymbol{r_1}, \boldsymbol{r_2} \ldots . \boldsymbol{r_n})$ which contains *3N* variables.

Hohenberg-Kohn derived two theorems as follows:

a) The ground state energy depends only on ***n(r),*** which is a function of three variables only

b) The ground state density n_0 is the function that minimizes the total energy ***E = F(n(r))***

This means that to calculate the total Energy *E* in the ground state, only the electron density is required. ~~This does not hold for excited states by definition of the Hohenberg-Kohn theorems above.~~

Utilizing the two Hohenberg-Kohn theorems above, Kohn-Sham derived a form for the energy functional as described below.

The functional $F(\boldsymbol{n}(\boldsymbol{r}))$ can be written as following:

$$E = F(\boldsymbol{n}(\boldsymbol{r})) = \int dr\, n(r) V_n(r) - \sum_i \int dr\, \phi_i^*(r) \frac{\nabla^2}{2} \phi_i(r) + \frac{1}{2} \iint dr dr' \frac{n(r) n(r')}{|r - r'|} + E_{xc}(n), \quad (17)$$

where the first term is the external potential, the second term the kinetic energy, the third term the Hartree energy and the last term $E_{xc}(n)$, the exchange correlation (*XC*) energy.

The last term, the exchange correlation (*XC*) energy, contains everything that is left out.

The ground state density n_0 is the function that minimizes the total energy ***E = F(n),*** as per Hohenberg-Kohn,

$$\frac{\delta F(n(r))}{\delta n(r)}|_{n_0} = 0. \quad (18)$$

This leads to *Equation (9)* with the additional term $V_{xc}(r)$, which includes the exchange (Fock) potential and the correlation potential:

$$\left(-\frac{1}{2}\nabla^2 + V_n(r) + V_H(R) + V_{xc}(r)\right)\phi_i(r) = \varepsilon_i\phi_i(r). \qquad (19)$$

The set of equations above are called the Kohn-Sham equations.

The additional term V_{xc} is given by:

$$V_{xc}(r) = \frac{\delta E_{xc}(n(r))}{\delta n(r)}|_{n(r)}, \qquad (20)$$

and is called the Exchange and Correlation Potential, which is a non-local function, which complicates substantially the application of the Kohn-Sham equations.

In order to model the ground state of a material we need to find good approximations for E_{xc}.and the so called local density approximation is the first and most commonly used approximation.

2.2.7 Local Density Approximation (LDA)

An approximation for E_{xc} can be made using a homogeneous electron gas as the basis for the calculation. [33]

In the free electron gas, it is assumed that the electrons do not interact with each other, and the potential due to the nuclei is constant.

It can be shown that the physical properties of the free electron gas depend on a single parameter, the electron density *n*, given by,

$$n = N/V, \qquad (21)$$

where *N* is the number of electrons and *V* the volume containing them.

There is a simple algebraic equation (not shown here), for the exchange energy of a free electron gas which is a function of N and V alone, for the free electron gas.

The correlation energy, for a specific value of electron density n(***r)*** in a free electron gas, cannot be described by a simple algebraic equation, but by solving the many-body Schrodinger equation numerically for the free electron gas, and removing the known kinetic, Hartree and exchange contribution (for the free electron gas these terms can be calculated), the correlation energy is left as the difference.

An approximation for the exchange and correlation energy in the simulated material, can be obtained from the free electron *n* and *V*, in Equation (21), as described below.

We take an electron density n(***r***) in an infinitesimal volume element ***dr*** of the simulated material and match this electron density to the same electron density value, i.e., n(***r***) at ***dr*** in the simulated material equals the value (or within a tolerance range) of N/V in a free electron gas. Then at this value (or range) of n(***r)*** for the free electron gas the exchange and correlation energies are obtained for the free electron gas. Note: n(***r***) for the simulated solid is required for this approach, but n(***r***) is a function of the exchange and correlation energy. A self-consistent calculation approach is required, that starts with initial approximations to n(***r***) in the simulated solid, and then improves these approximations through subsequent iterations, as described in section 6.2.11.

Each volume element ***dr*** in the solid can be represented with a density, ***n(r)*** at that element and the contribution to exchange energy dE_{xc}at that element is,

$$dE_{xc} = \frac{E_{xc}^{HEG}[n(\boldsymbol{r})]}{V} d\boldsymbol{r}, \qquad (22)$$

where *HEG* means Homogeneous Electron Gas and $E_{xc}^{HEG}[n(\boldsymbol{r})]$ is calculated (i.e., the value for the free electron gas at the density ***n(r))*** for ***n(r)*** at ***dr,*** where ***dr*** references a differential unit of volume).

Summing over the volume of the solid will then give the total exchange correlation energy E_{xc}. [33].

2.2.8 Plane Wave Expansion for Numerical Simulation

The solution $\Psi\ (\boldsymbol{r_1}, \ldots \ldots \boldsymbol{r_n}) = \ \phi_1\ (\boldsymbol{r_1}) \ldots \times \ldots \phi_n\ (\boldsymbol{r_n})$, to the many-body Schrodinger equation, *Equation (1)* can be represented as a Fourier series (for each $\phi_I\ (\boldsymbol{r_i})$) with the wave vectors ***k*** of each term representing the harmonics of the series for each $\phi_I\ (\boldsymbol{r_i})$.

The Bloch Theorem imposes a condition on the wavefunction for a periodic solid. It states that the wave function is a product of a function with the periodicity of the lattice of the periodic solid and a plane wave (with wave vector, denoted as ***k*** in the following). It turns out that many parts of the DFT equations are easier to solve using the wave vector ***k***, than using the position vector ***r***. Solutions of this form take the name plane wave solutions.

The Bloch Theorem for an electron wave function φ in a periodic potential can be stated as,

$$\varphi_{j,k} = u_j \circ e^{i\boldsymbol{k}\cdot\boldsymbol{r}}, \tag{23}$$

where u_j (**r**) is a function that has the periodicity of the potential in the crystal lattice, i.e.

$$u_j\ (\mathbf{r} + \mathbf{R}) = u_j\ (\mathbf{r}), \tag{24}$$

with ***R*** representing the crystal lattice vector positions.

Therefore *Equation (23)* can be described as a product of a periodic function of the lattice and a plane wave with wave vector ***k***. Then as u_j is periodic with the periodicity of the crystal lattice (24), it can be represented as a Fourier series (25),

$$u_j\ (\boldsymbol{r}) = \sum_{\boldsymbol{G}} c_{j,G} e^{i\boldsymbol{G}\cdot\boldsymbol{r}}\ , \tag{25}$$

where the ***G*** represent the wave vectors for each harmonic. As the function is periodic in the crystal lattice, the ***G*** are given by the vectors of the reciprocal lattice positions (i.e., geometry with units of 1/distance and geometry described by $\boldsymbol{G} = \frac{2\pi}{\boldsymbol{R}}$) .

The wave equation for an electron can then be written as:

$$\varphi_{j,k}(\boldsymbol{r}) = \sum_{\boldsymbol{G}} c_{j,k+G} e^{i(\boldsymbol{k}+\boldsymbol{G})\cdot\boldsymbol{r}}. \quad (26)$$

In order to find these wave functions numerically the values of the wave vectors ***k*** and their coefficients need to be added as input to the simulation.

In order to keep computation time within reasonable limits there are methods to choose the ***k*** which will be used as input to the numerical solution, therefore restricting the actual number of ***k*** (called ***k***-point sampling) used as input to the model (see, e.g., [29]).

2.2.9 *k*-Point Sampling for Input to the Numerical Solution

The symmetry of the reciprocal lattice (as a result of the symmetry of the real lattice (24)), results in some wavevectors ***k***, being equivalent (due to symmetry) and therefore not required as distinct terms in the Fourier series expansion of the solution, see *Figure 7*.

For a periodic lattice, [34], describes how only the wave vectors in the first Brillion Zone of the reciprocal lattice represent unique harmonics in the Fourier series of the wave equation (i.e., the plane wave expansion of the wave equation for an electron, requires only those wave vectors ***k*** in the first Brillion Zone of the reciprocal lattice).

This still results in a possible large number of wave vectors ***k*,** (the actual number is the volume of the solid under consideration divided by the number of unit cells in that volume, [34]). Strictly speaking, this is a finite number, but in reality is treated as infinite and an integral formulation would be required for any summation involving all of these ***k***-points. A further reduction in the number of ***k***-points used is required for use in the model.

Since the electron wave functions will be almost identical for values of ***k*** that are sufficiently close, one can represent the wave functions over a smaller region of reciprocal space by considering the wavefunction at a single ***k***-point for that region, and therefore taking discrete as opposed to continuous values as input to the model.

Further to this selection we can use a smaller number of ***k***-points, by using weights for the discrete points sampled where the weights relate to symmetry of the ***k***-points within the reciprocal lattice geometry (i.e. ***k***-points with high symmetry have higher weights, see *Figure 7*).

A periodic function of the real lattice $f(\boldsymbol{r})$ can then be approximated by a series of weighted terms with wave vectors as shown below;

$$f(\boldsymbol{r}) = \frac{\Omega}{(2\pi)^3}\int_{BZ} F(\boldsymbol{k})d\boldsymbol{k} = \sum_j \omega_j F\left(\boldsymbol{k}_j\right), \qquad (27)$$

where *F(**k**)* is the Fourier transform of $f(\boldsymbol{r})$, Ω is the cell volume and the ω_j are weighting factors.

The set of sample ***k***-points chosen to appropriately sample the Brillouin zone can be obtained via various standard methods, in this case we use the Monkhorst-Pack method. [35]

The ***k***-points are distributed through reciprocal space as

$$\boldsymbol{k}_j = x_1\boldsymbol{b}_1 + x_2\boldsymbol{b}_2 + x_3\boldsymbol{b}_3, \qquad (28)$$

where the $\boldsymbol{b}_i$ are reciprocal lattice vectors, and

$$x_{ij} = \frac{l_i}{n_j}, \qquad (29)$$

where the l_i are lengths of reciprocal lattice vectors, and n_j is an integer determining the number of special points in the set, and *j = 1…*n_j

An example of 3D Brillouin zone (BZ) for face-centered cubic (FCC) crystal is depicted in *Figure 7* below. Gamma Point *Γ*, which is used to reference (0, 0, 0) is shown and other points of high symmetry are marked. The symmetry of a point will impact the weighting given in the above equation (27). This BZ (its irreducible part) has been used to calculate the bulk properties of the Si crystal, such as the phonon spectra, and the bulk density of stated and optical response which will be compared with its surface counterparts.

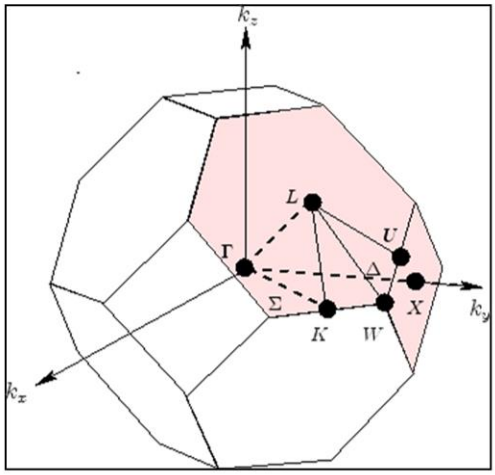

*Figure 7. High symmetry **k**-Points of the Brillouin Zone (BCC) for the FCC Cubic Lattice.*

We also model the surface (as opposed to the bulk), which can be represented as a 2d-Brillouin Zone for electrons that will be located in the surface only. The surface 2d Brillouin Zone is a projection from the underlying 3d-Brillioun Zone of the bulk as depicted in *Figure 8* below. As with the bulk high symmetry ***k*-**points can be selected as input to the numerical model.

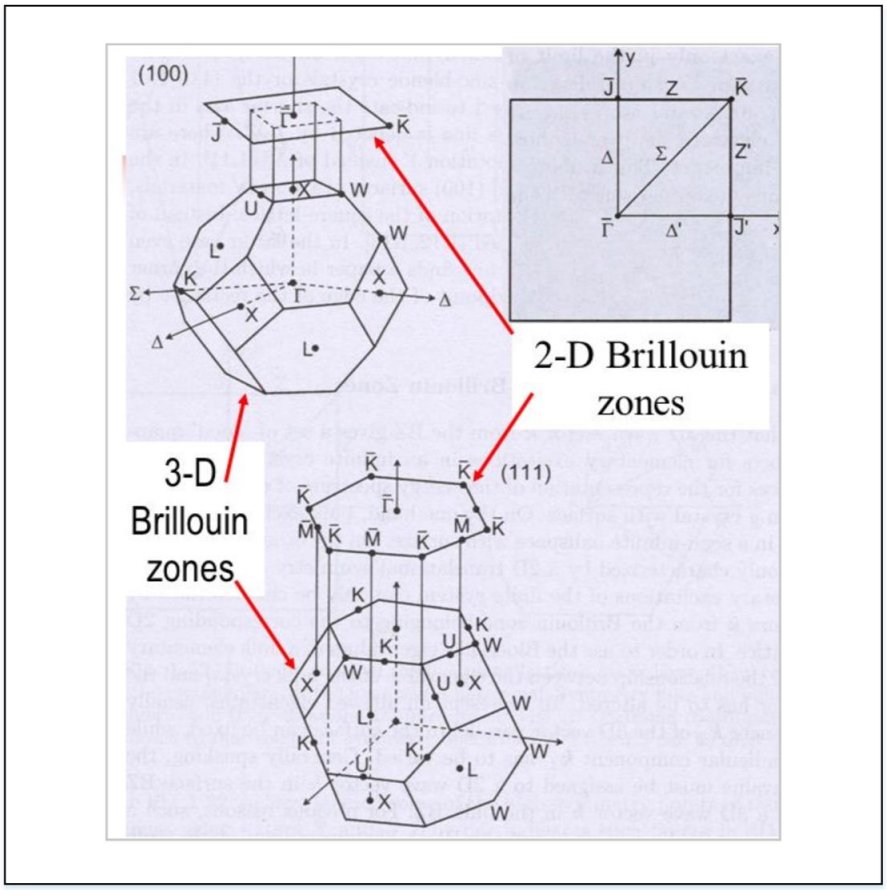

*Figure 8. High symmetry **k**-points projected to the FCC (100) surface (top), FCC (111) Surface (bottom).*

One further consideration is required. The kinetic energy of the electron is given by the left-hand side of (30) below,

$$\frac{\hbar^2}{2m}\,|\boldsymbol{k}+\boldsymbol{G}|^2 \rightarrow E_{cut}\,. \qquad (30)$$

We need to cut off the summation of plane waves at some point for the numerical calculation. (i.e., we have an infinite number of $\boldsymbol{G}$ that we could sum over)

To limit this we use the energy, E_{cut} as a cut-off parameter as input to the simulation. This parameter can be tuned to a value appropriate for the specific requirements of the simulation.

2.2.10 Pseudo Potential

The majority of physical properties of solids depend upon the valence electrons. Taking Si as an example, the core states, 1s, 2s and 2p are tightly bound to the nucleus, with their charge densities peaking below 1 Bohr distance from the nucleus, whereas the valence states 3s and 3p have a peak charge density approximately at a distance of half the Si-Si bond length (approximately 2 Bohrs) from the nucleus. The valence states are therefore more sensitive to changes in the chemical bonding environment.

In order to simplify the computation by avoiding deeply located electron states with strongly oscillating wave functions, we can partition the electrons between core and valence states. The core states are held frozen, as they are for a single atom. The Kohn-Sham wavefunctions are then not required for these states which can lead to a large computational saving.

Therefore, the core electrons and ionic potential are replaced with a smooth *pseudopotential* (effective potential). This effective potential is used in the Schrodinger Equation and along with the plane wave expansion method, described earlier. This results in fewer harmonics being required to describe the wave function of the system and smaller number of electrons to be considered.

The procedure to obtain the new Pseudo Potential is as follows;

- Calculate the Kohn-Sham wavefunction with the core electrons present
- Decide on a radial cut-off, r_c, that is the radius that sets the boundary of where the wavefunction will be modified. The region 0 -> r_c is where the wavefunction will be modified, the “pseudo region”
- Inside the “pseudo region” replace the wavefunction by a smooth polynomial. See Ψ_{pseudo} in *Figure 9*
- The new function is chosen to yield the same electron density as the replaced function in the “pseudo region”, and will be a polynomial of equal or lower order than the function it is replacing. The replaced function will also need to match the original function value and slope at *r* = r_c
- The new smooth wavefunction will have the same Kohn-Sham eigenvalue as the original function.

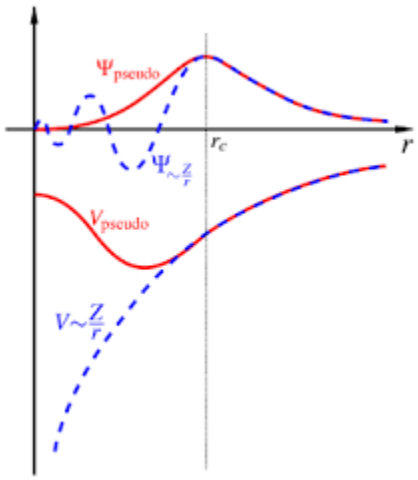

Figure 9. Pseudo potential concept is described in the graph. A new potential V_{pseudo} (red) is created using a modified wavefunction Ψ_{pseudo} in the "pseudo region" as discussed above.

As depicted in *Figure 9*, a radial boundary r_c is decided upon that defines the region (in *Figure 9* this region being defined on the *r* axis from zero to r_c) that will have a pseudo potential defined, as discussed above. [29]. When performing MD simulations at high temperatures one has to make sure that the instantaneous distance between the atoms (Si in our case) is larger than $2 \cdot r_c$. To avoid this problem we used the so called "hard-core" pseudopotential, which has r_c sufficiently small to avoid the core overlap during the dynamics.

2.2.11 Self-Consistent Calculations

Self-consistent calculations are used in the numerical simulations. An example of the technique is given here, in this case to find the electron ground state energy of the Si slab under consideration from the Kohn-Sham equations below.

$$\left(-\frac{1}{2}\nabla^2 + V_n(\boldsymbol{r}) + V_H(\boldsymbol{r}) + V_{xc}(r)\right)\phi_i(r) = \varepsilon_i\phi_i(\boldsymbol{r}), \qquad (31)$$

$$V_n(\boldsymbol{r}) = \sum_{i,I} \frac{Z_i}{|r_i - R_I|}, \quad (32)$$

$$V_{xc}(\boldsymbol{r}) = \frac{\delta E_{xc}(n)}{\delta n}|_{n(r)}\ , \quad (33)$$

$$\nabla^2 V_H(\boldsymbol{r}) = -4\pi \mathrm{n}(\mathbf{r}), \quad (34)$$

$$\mathrm{n}(\mathbf{r}) = \sum_i |\phi_i(\boldsymbol{r})|^2. \quad (35)$$

The problem is that the values of the variables in all the equations depend upon each other and therefore there is no obvious way to initiate the numerical solution to the equations, given that the values of the variables in the equations are not known a-priori.

A method to solve this is to estimate the initial value of some of the variables, enough to get an initial solution to (31), and then using the solution to (31) recalculate the values of the initial variables and continue doing this in a loop until the difference between the previous value of the variables (the previous loop) and the new value is within some agreed tolerance. This is the origin of the name self-consistent as the process is continued until the previous and current values of the variables are consistent within a tolerance to each other. The tolerance is defined by the accuracy of the simulations required.

Specifically, in the case above the initial variables that can be approximated (not discussed here how these approximations are obtained, but available in standard literature [29]) are the potentials used in (31).

Therefore, an initial approximation for *n(**r**)* and $V_n(\boldsymbol{r})$ can be used in (31). Depending on the systems, it is often convenient to start with atomic wave function, which are known from the pseudopotential calculation, (several types of the pseudopotential for each element in the periodic table of the elements are available). Then the $\phi_i(\boldsymbol{r})$ obtained can be used in (35) to find

a new value of ***n(r),*** which is then compared to the previous value to see if the difference is within tolerance. This process is continued until the difference is within the tolerance specified. At this point the solution is assumed to be in the electronic ground state, and can be used to obtain *E* the energy of the ground state.

2.2.12 Equilibrium Configuration and Hellman – Feynman Theorem

In order to obtain the equilibrium configuration for the crystal, repeated slab, or other system, both nuclei and electrons are modelled, but the nuclei are treated classically. This section gives more detail on how this is achieved.

As the nuclei motion is much more constrained and slower than that of the electrons the wave function of the nuclei can be split from that of the electrons as below

$$\Psi\,(r_1 \ldots\ldots r_n, R_1 \ldots\ldots R_n) = \Psi_R(r_1 \ldots\ldots r_n)\Upsilon(R_1 \ldots\ldots R_n). \qquad (36)$$

The electronic wave function $\Psi_R(parametric\ dependence\ on\ the\ nuclear\ coordinates\ R)$ is determined first for a fixed set of nuclear coordinates $(R_1 \ldots\ldots R_n)$, and then the nuclear wave function is determined.

It is possible to write the Schrodinger equation with only the nuclear wave function explicitly shown as below

$$[\sum_I \frac{\nabla_i^2}{2M_I} - \frac{1}{2}\sum_{I\neq J}\frac{Z_I Z_J}{|R_I - R_J|})\,\psi + \mathsf{E}(R_1 \ldots\ldots R_n)]\,\Upsilon = E_{tot}\Upsilon, \qquad (37)$$

where the effect of the electrons is contained within the term $E(R_1 \ldots\ldots R_n)$, which acts as an effective potential for the nuclei (note: we also have the Schrodinger equation for electrons only as detailed in an earlier section).

The separation of the Schrodinger equation into two equations (electronic and nuclear) is termed the Born-Oppenheimer approximation, as mentioned earlier.

From (37) we can describe a nuclear Hamiltonian as,

$$H_n = -\sum_I \frac{\nabla_i^2}{2M_I} + \mathrm{U}(R_1 \ldots\ldots R_n), \quad (38)$$

where the total potential energy of the nuclei is given as,

$$\mathrm{U}(R_1 \ldots\ldots R_n) = \frac{1}{2} \sum_{I \neq J} \frac{Z_I Z_J}{|R_I - R_J|} + \mathrm{E}(R_1 \ldots\ldots R_n). \quad (39)$$

The next step is to treat the nuclei classically. In this manner the quantum mechanical momentum operator can be replaced by the classical momentum $\boldsymbol{P}_I$, obtaining the classical Hamiltonian for the nuclei,

$$H_n^{class} = \sum_I \frac{\boldsymbol{P}_I^{\,2}}{2M_I} + \mathrm{U}(R_1 \ldots\ldots R_n), \quad (40)$$

and by Hamilton's equations of motion the below can be derived:

$$F_I = \frac{\delta U}{\delta R_I}, \quad (41)$$

where F_I is the force on the nuclei.

Therefore, the equilibrium structure of the slab will correspond to the minimum of the function $U(R_1 \ldots\ldots R_n)$, which is termed the potential energy surface.

However, the calculation of the electronic energy $E(R_1 \ldots\ldots R_n)$ for each nuclear configuration would be prohibitively time consuming.

The Hellman-Feynman theory states that we can obtain F_I for all nuclear coordinates by using the electron density *n(**r**)* for one set of nuclear coordinates only as below

$$F_I = Z_I \left[\int n(\boldsymbol{r}) dr \, \frac{r - R_I}{|r - R_I|^3} - \sum_{J \neq I} Z_J \frac{R_J - R_I}{|R_J - R_I|^3}\right], \qquad (42)$$

i.e., *n(**r**)* only required for ONE set of nuclear coordinates.

Therefore, the electron ground state density *n(**r**)* can be obtained as previously described by a self-consistent calculation and then *Equation (42)* is employed to find the nuclear forces. Various standard numerical methods can be used to find the total energy minimum by following the directions of these forces, such as steepest descent, conjugate gradients etc. [29]

2.2.13 Density Functional Theory Limitations

DFT as described can be used with good accuracy to obtain the ground state properties of the collection of atoms, including equilibrium atomic structures, vibrational properties and structural phase transitions, band structures of metals and semiconductors for the filled electron states (valence band) as well as calculation of interatomic forces. In principle, DFT is an exact ground state theory, but this is not the case when the excited states have to be considered.

Additional techniques have to be applied to DFT to accurately calculate crystal properties, which are related to the excited electronic states (those in the conductivity band) such as optical properties and electronic bandgaps of semiconductors. The standard (and substantially more CPU demanding) approach to correct the underestimation of the transition energies is using Green's function approach within the GW approximation [29]. The simple, but reasonably effective so-called scissors-operator approach, can be applied if necessary, to correct a DFT-LDA that is lower than the experimental energy gap. It simply shifts energies of all the excited states by the same amount, for the Si crystal it is usually about 0.7 eV, although its value also depends on the choice of the pseudopotential. In our calculations we used a DFT-LDA energy gap without applying the scissors corrections: even though the scissors corrections are widely used, their application still has to be tested for each specific case.

3 Numerical Formalisms (used for this thesis)

To derive the results in this thesis various formalisms were used, all based upon DFT. This section describes in more detail these formalisms. *Table 4* in the theoretical results section also indicates which formalisms were required for each result presented.

3.1 *Car-Parrinello Molecular Dynamics (CPMD)*

The first principles Car-Parrinello molecular dynamics simulation requires the ground state energy of a crystal or the slab as input, derived by Density Functional Theory (DFT) as described in previous sections and [29].

The first step in the CPMD simulation is an electronic minimization to bring the system to the ground state, utilizing the DFT techniques already discussed, and the ground state energy of the slab thus minimized, is used as input to the start for the molecular dynamics simulation.

During the molecular dynamics simulation, the nuclei are assumed to move classically, with the use of an extended Lagrangian that couples equations for the electrons and nuclei, allowing for simultaneous solutions for both electrons and nuclei. Unlike the BOMD [58], there is no electronic minimization at each step of the molecular dynamics simulation, which makes the CPMD substantially more CPU efficient. And CPMD uses the plane wave expansion at the gamma point only for the Brillouin zone (by default the CPMD application requires a bigger supercell) and the pseudopotential implementation of DFT.

For the Car-Parrinello simulations Gamma (Γ) Point (0,0,0) is used as the only ***k***-Point. Since in our particular case the supercell contains eight primitive Si(100) surface cells, one Gamma Point is equivalent to eight ***k***-points in the primitive unit cell, which brings sufficiently accurate surface BZ sampling. An Energy cut-off of 12Ry is used, which produces well converged structural and electron properties for the silicon atoms.

3.2 *Born Oppenheimer Molecular Dynamics (BOMD)*

The BO molecular dynamics simulation requires the ground state energy of the slab as input, derived by Density Functional Theory (DFT) as described in previous sections.

The first step in the BOMD simulation is an electronic minimization to bring the system to the ground state, utilizing the DFT techniques already discussed, and the ground state slab thus obtained, is used as input to the model for the dynamics simulation.

During the dynamics simulation, the nuclei are assumed to move classically, the nuclear positions are kept constant while the electronic Schrodinger Equation is solved. Then Hellman Feynman theorem is used to obtain the average nuclear potential and forces, which modify the nuclear coordinates according to the forces, and then the simulations are continued in order to obtain the new potential energy surface. Therefore, unlike CPMD, BOMD performs an electronic minimization at each step of the MD run. We used BOMD for the same supercell to check our dynamical results, obtained from CPMS. Also, BOMD is required to calculate the band structure and optical response with the use of a large number of ***k***-points. In this case the atoms are fixed in their positions.

Parameters used in this thesis when running BOMD simulation

The number of input ***k***-points used in self-consistent (SCF) part of the simulations, which calculates the electron charge density and potential, is two. The coordinates for these two special ***k***-points in reciprocal space are given in the *Table 2* below;

K-Point	**X-Coord**	**Y-Coord**	**Z-Coord**
k(1)	0.2500000	0.5000000	0.2083333
k(2)	0.2500000	-0.5000000	-0.2083333

Table 2. ***k***-points used for BOMD.

After the potential and the ground charge density is determined by the SCF method, for the non-self-consistent (NSCF) simulation mode for the optical properties and DOS calculations, a homogeneous grid of 32 × 32 =1024 ***k*****-**points was used.

An energy cut-off of 12 Ry is used, for all the simulations, including phonon, CPMD and BOMD.

3.3 *Density Functional Perturbation Theory (Phonons)*

As part of this thesis we use a technique to obtain phonon responses of the Si(100) surface at a range of frequencies. However, to calculate phonon spectra at arbitrary wavevector points a standard perturbation approach to DFT can require a large computational effort. New formalism

termed Density Functional Perturbation Theory (DFPT) [36] has been developed to address this issue.

The two main formalisms of DFPT are due to Baroni [27] and Gonze [58]; although the two may be shown to be equivalent, there are differences in the implementation that may result in one method being preferable to another. The Baroni formalism is centered upon obtaining a series of equations that may be solved self-consistently using Green's function methods; the Gonze formalism is based rather upon a perturbative expansion of the Kohn-Sham energy functional, leading to a variational problem for even orders of expansion akin to the zeroth order problem.

This theory and technique is quite involved and is not discussed here. See [27] for further information. We used the Baroni formalism on this thesis, this formalism has been implemented as a part of the Quantum Espresso package.

3.4 *Linear Optical Response – (DFT based EPSI Program)*

For the simulation to obtain the linear optical response, that is the dielectric function *ε(ω)* of the Si(100) surface within the repeated slab method, the excited states have to be included. The calculational approach used is based upon DFT, but additional techniques are required. A brief summary of the theory behind the additional techniques is given below.

The dielectric function of Si cubic bulk is isotropic, so the dielectric tensor contains only three equal diagonal elements for the bulk, i.e.,

$$\varepsilon_2^{ii} = \varepsilon_{xx} = \varepsilon_{yy} = \varepsilon_{zz} \ ,$$

and the imaginary part of the dielectric function is calculated by evaluating the expression:

$$\varepsilon_2^{ii}(\omega) = \frac{\hbar^2 e^2}{\pi \omega^2 m^2} \sum_{vc} \int_k d\boldsymbol{k} \quad p_{vc}^i(\boldsymbol{k}) p_{cv}^i(\boldsymbol{k}) \delta\left(E_c(\boldsymbol{k}) - E_v(\boldsymbol{k}) - h\upsilon\right), \qquad (43)$$

where *v* and *c* label valence and conduction states of energy $E_v(\boldsymbol{k})$, $E_c(\boldsymbol{k})$ respectively, ω is the angular frequency of the photons, and *m* and *e* are the electron mass and charge,

and,

$p_{cv}^{i} = < c, \boldsymbol{k} | p^{i} | v, \boldsymbol{k} >$ is the matrix element of the momentum operator ***p*** between the empty and filled states.

Since the Si(100) surface with dimer reconstruction is clearly anisotropic structurally, one should expect different components at ε_{xx}, $\varepsilon_{yy}, \varepsilon_{zz}$. We will demonstrate that this is the case, such anisotropy defines the Reflectance Anisotropy experimental technique. Only transitions from the filled Kohn-Sham states to empty Kohn-Shan states can contribute to the absorption of light and in these transitions the wavevector of the initial state, $u_{v\boldsymbol{k}}$ must be equal to the wavevector of the final state $u_{c\boldsymbol{k}}$, that is the transitions are vertical in ***k***-space. Only transitions where the energy difference between the energy of the empty state $\varepsilon_{c\boldsymbol{k}}$ and that of the occupied state $\varepsilon_{v\boldsymbol{k}}$ equals the energy of one photon, $\hbar\omega$ can contribute to the optical absorption by the material and the energy onset of the optical absorption corresponds to the smallest energy difference $\varepsilon_{c\boldsymbol{k}}$ – $\varepsilon_{v\boldsymbol{k}}$, between conduction and valence states with the same wavevector, i.e., to the direct bandgap.

For further details of the formalism and its applications see [37] , [38].

For the linear optical response simulations used in this thesis, 1024 ***k***-points, homogeneously distributed along the surface BZ, were used, while a Monkhorst-Pack approach has been used to determine the self-consistent potential.

4 Structural Details of the Si(100) repeated Slab, used as input to the Simulations

The Si(100) structure is modeled by the slab as described below.

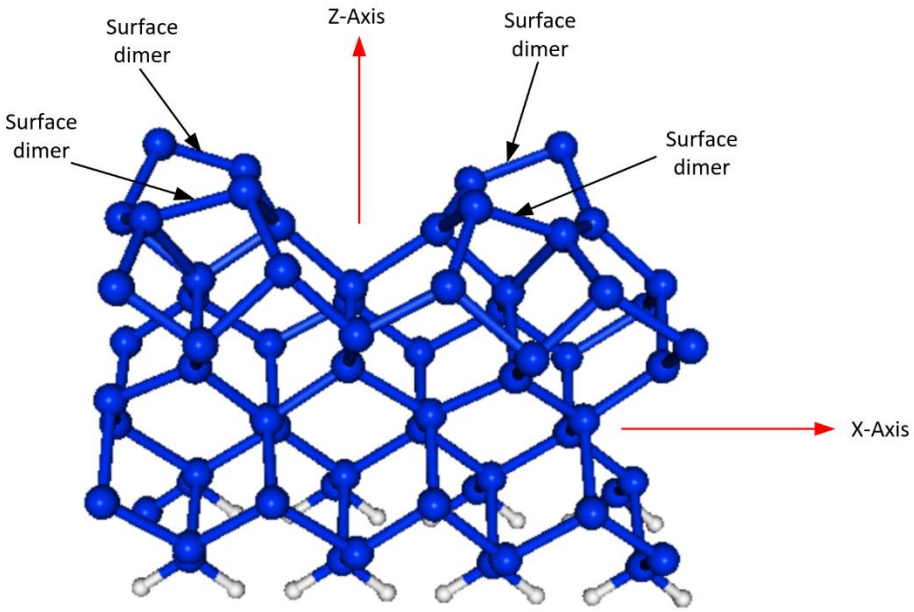

Figure 10. Ground state (that is at zero temperature) Si(100) c(4×2) reconstructed super cell, perspective view. It contains four p(2×1) building blocks, 8 layer-thick and 8 Si atoms for every layer (blue balls) can be seen. Therefore, the slab contains 64 Si atoms. The surface dimers are annotated at the top of the diagram. The white balls at the bottom are H atoms in fixed positions, used to preserve the slab bottom in the bulk-like configuration.

A 64 Si atom supercell is used in the simulations, see *Figure 10*. There are 8 layers, each contains 8 Si Atoms. The supercell, therefore, contains eight Si(100)(1×1) units, compatible with two main surface reconstructions, namely p(2×2) and c(4×2). To preserve the bulk-like environment of the slab, the lowest Si layer is fixed in an ideal position. This layer has been saturated with 16 fixed H atoms used as the base of the supercell. The dimers at the surface are annotated in this figure. With this supercell there are four dimers at the surface (a total of 8 Si atoms).

Most of the molecular dynamic simulation runs were started with a supercell in the Si(100) p(2×2) configuration. The starting temperature for the supercell is simulated by randomizing the Si atom positions in the supercell by a configured amount (based upon the desired supercell

temperature) prior to running the molecular simulation. Typically, a few thousand steps of the MD run is necessary to get the equilibrated atomic vibrations.

The supercell dimensions are given in *Table 3* below:

Dimension	**Length**
X - Axis	29.02 au
Y - Axis	0.5 × 29.02 au
Z - Axis	1.2 × 29.02 au
Vacuum	8 Angstrom

Table 3. Supercell dimensions, used for most of the Si(100) simulations in the thesis.

Here the Z-axis, perpendicular to the Si(100) surface is in the plane of the paper for *Figure 10,* and points upwards.

In order to mimic a semi-infinite crystal, confined by (100) oriented plane, for the model, we replicate the supercell in all dimensions and assume periodic boundary conditions (PBC). This gives a periodicity to any physical quantity in the supercell and allow use of the Fourier expansion in all three dimensions.

The solutions to the Schrodinger Equation are obtained via a plane wave expansion of the solution to obtain the Fourier Coefficients of specific harmonics. The maximum number of harmonics calculated is determined by the cutoff energy used in the simulation.

Using the Brillouin Zone of the supercell specific ***k***-Points can be selected for simulation based upon symmetry of the Brillouin Zone, as an example see *Figure 7* and *Figure 8*. For this thesis the CPMD method uses only Gamma Point, and for the BOMD runs we used two ***k***-points as described in *Table 2*. For the Optics simulations 1024 ***k***-Points were used.

To create a sample supercell for Si(100) surface at a temperature higher than 0K, we used randomization of the atomic positions, i.e., the bonds can be randomly extended or contracted within a certain range. The amount of randomization determines the MD temperature of the slab and in this manner various starting temperatures for molecular dynamics runs can be set.

For the temperature dependent optical response simulations we considered several (up to four) representative instantaneous configurations of the supercell. These configurations were taken from various points in the run of the molecular dynamics simulations. Such an approach mimics the experimental temperature dependent optical response, based on the ergodic theorem.

5 Theoretical Results

This section contains a general introduction to the results (section 5.1), and then four subsections detailing the results obtained. Three of the sub sections detail the results for Molecular Dynamics, Phonon Response (calculated phonon spectra) and the Linear Optical Response respectively. Section 5.1.4 provides a summary table for all of the results.

5.1 *Results and Discussion*

Study on the surface reconstructions of the atomically clean silicon (100) surface can be traced back to the year 1959 when a Si(100) p(2×1) pattern was observed by Schlier and Farnsworth with the low energy electron diffraction (LEED) technique [39]. The authors argued that this was caused by the top surface atoms moving together in pairs to saturate the dangling bonds at the ideally terminated Si(100), and form new bonds, called dimers [39] (see *Figure 3*). The formation of surface dimers would remove one of the two dangling bonds per surface atom without necessarily changing any surface bond lengths by more than a few percent.

Since then the properties of the Si(100) surface have been extensively studied due to the impact of that surface in modern microelectronics. For instance, Si(100) surface based devices are the main components of CPU and RAM in modern microelectronics.

Dimerization, as the basic clean Si(100) reconstruction mechanism, has been used in interpreting LEED, photoemission, ion channeling, optical absorption, electron energy loss, and core-level spectroscopy experiments [40]. Dimers have been also observed directly by scanning tunneling microscopy (STM). Different reconstruction patterns have since been observed for the Si(100) surface. At low temperature c(4×2) has been found in LEED experiments, see, e.g., [8]. The symmetric p(2×1) dimer pattern has been observed by scanning tunneling microscopy (STM) at room temperature [16,19]. However, the low temperature STM imaging reveals the higher-order p(2×2) and c(4×2) reconstructions [16]. It was suggested that the nonzero temperature dynamics of the top atoms is responsible for the temperature dependent modification of the Si(100) reconstruction, or the p(2×1) appearance in various spectroscopies.

Si(100) dynamics has been investigated both theoretically and experimentally (see, e.g., Uda, et al. [6]). Even though a wide range of temperatures have been employed both in experimental characterization and surface growth, most of the structural and optical properties were calculated at absolute zero temperature [9] [41]. For the semiconductor surface, however, temperature modification of the atomic vibration and optical response should be more pronounced than for the bulk due to surface atom reduced coordination, symmetry change and

reconstruction. This has to be included in the surface optical formalism and this is a part of the goal of the thesis.

To explicitly incorporate the temperature dependent bulk dynamics, Z. A. Ibrahim, et al., [40,44] developed a formalism for temperature dependent dielectric functions of bulk semiconductors and compared the calculated dynamically modified optical response with the experimental measurements for GaAs and Si bulk. It was demonstrated that the molecular dynamics, combined with the optical response simulations allows us to accurately reproduce the temperature dependent optical broadening and the optical peaks shift.

In the numerical results presented next in the thesis we apply the above combined computational approach to investigate the dimer dynamics of the clean Si(100) surface and the contribution of the thermal motion effects on the reflectance (RA) spectra of the clean Si(100) surface in a wide temperature range. Even though, more temperatures have to be simulated, our results are proving that its possible to successfully incorporate the dynamical effects in the optical theory and get more detailed access into the Si(100) surface structure.

5.1.1 Theoretical Results on Molecular Dynamics

Finite temperature Car-Parrinello Molecular Dynamics (CPMD) has been used to simulate temperature dependent modification of the microscopic Si(100) dimer structure. We use a periodically repeated slab made up of eight layers of Si(100), each containing eight atoms. In the bottom plane the Si dangling bonds are saturated with 16 hydrogen atoms. The vacuum thickness of the slab, required to avoid spurious overlap of the repeated slab surfaces, was 8 Angstrom. At the surface plane the supercell with eight atoms per layer is p(4×2) allowing unbiased access to the main reconstructions, namely p(2×2), c(4×2) and (2×1). During both relaxation and dynamics the top five layers of Si were allowed to move, while the sixth Si layer and the bottom H layers were fixed in the bulk like position. The kinetic energy cutoff in the plane wave expansion of the electronic wave functions was 12 Ry, which is sufficient to get well converged results in the surface atomic structure.

As discussed below, the molecular dynamics at sufficiently high temperatures leads to the Si(100) dimers flipping, as a result of dynamical switching between the c(4×2) and p(2×2) structures. The corresponding ball and stick models of these two reconstructions within the supercell used in the simulation, are presented in *Figures [12, 13, 14]*.

The dynamics of the temperature dependent dimer motion can be conveniently described by plotting the time dependent difference in the vertical dimer positions. This representation of the dimer transformation is given in the following figures.

In *Figure 11*, the vertical dimer motion shifts are illustrated for a CPMD run at an average MD temperature of 580K. The results show a difference in the top atom shift along Z-axis, that is the (100) direction. The vertical positions difference (dynamical buckling) of the four dimers on the surface of the Si slab used in the run, are shown. For dimer 1 and 2 the flipping is observed at approximately 500fs and 750fs. For dimer 3 and 4 the flipping is observed at approximately 750fs and 1400fs. Note that there is no visible correlation between the dimer flipping in the adjacent rows, while in the same row the dimers switch simultaneously. That is also a dynamical confirmation that the p(2×1) symmetric phase is unstable with respect to formation of the higher order reconstructions. Dimer flipping results in two different reconstructions of the Si(100) surface. In this case we observed c(4×2) and p(2×2) reconstructions during the run.

It is clear that such frequent dimer flipping will result in apparent p(2×1) LEED or STM patterns, furthermore the STM image will correspond to the time-averaged symmetric-like arrangement of the top Si(100) atoms. This theoretical conclusion agrees with the experimental STM/LEED symmetric (2×1) dimer appearance results and the STM image simulation [43], even though the actual dimers are buckled.

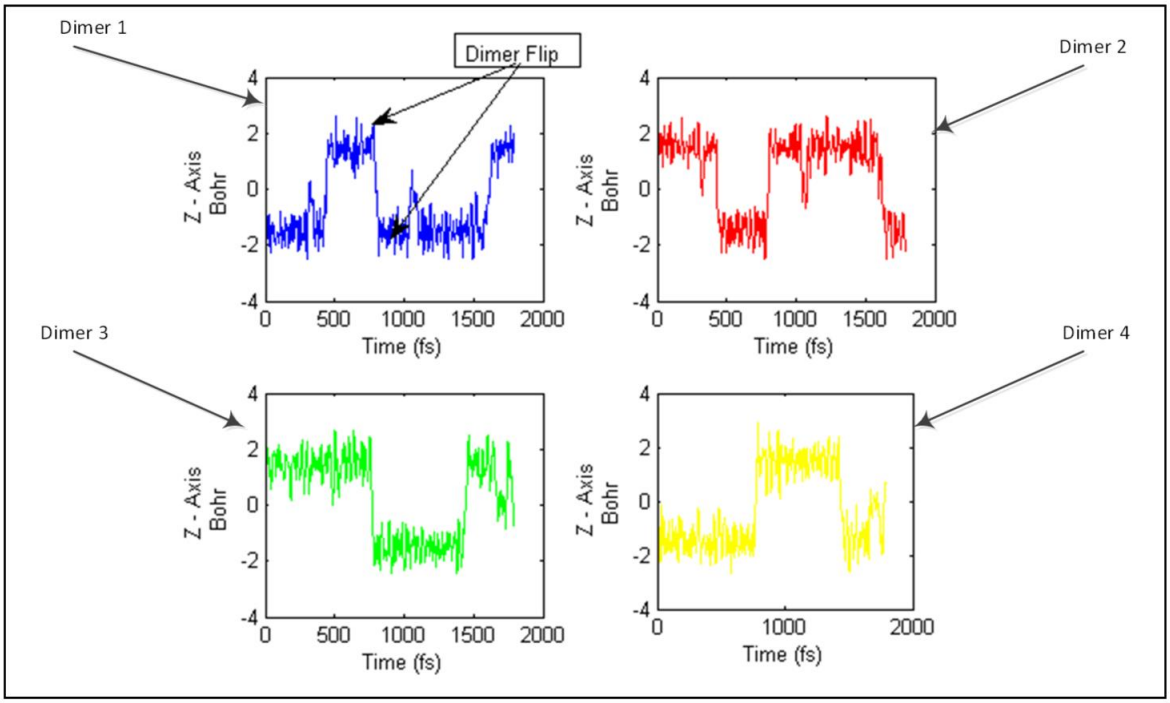

Figure 11. Dimer relative vertical displacement (along Z-axis) for the Si(100) surface, (units are Bohr) , at an average temperature of 580K for CPMD, input Si Slab is 580K p(2×2) has been randomized (to obtain the MD temperature of 580K) and used to start the simulations. All dimers exhibit dimer flipping, i.e., the relative Z-axis height for the dimer flips as depicted above.

At three time intervals through the run (600fs, 1000fs, 1500fs) the surface structure of the Si slab is depicted in *Figure 12, Figure 13*, and *Figure 14*. *Figure 12* shows a snapshot of the p(2×2) reconstruction, a similar configuration is shown in *Figure 13*, i.e., a p(2×2) reconstruction but with the two dimer pairs flipper in relation to the previous *Figure 12*. Finally, *Figure 14* depicts a dynamical snapshot with a c(4×2) configuration.

The appearance of buckled (rather than symmetric) dimers has been confirmed conclusively by simulating the reflectance anisotropy (RAS) of the Si(100) surface. It has been shown by A. Shkrebtii at al. that Si(100) 2x1 dimers are asymmetric [12]. Further results favor the asymmetric dimerization in a temperature range of 120K to 770K [10].

For many experimental and theoretical investigations the clean Si(100) is often represented as p(2x1) reconstructed. However, this is actually a dynamical mixture of c(4x2) and p(2x2) and the

"(2x1)-like" appearance is due to interesting dynamics with dimer flipping. The temperature dependent c(4×2) switching to p(2×2) and back produces an apparent (2x1) like surface [10].

As discussed, the c(4×2) and p(2×2) reconstructions at clean Si(100) are energetically very close. Additionally, the low potential barrier for dimer flipping (estimated to be within 0.03 - 0.11 eV [15], [44]) leads to the c(4×2) and p(2×2) structures switching: this energy barrier becomes comparable with the thermal excitation energy above a temperature of 200K. Actually, c(4×2) and p(2×2) are practically degenerate in energy, so both of them are equally probable at the ground state, they both exist and are stable at low temperature [10].

In STM experiments at 120K, c(4×2) is the dominant component observed [44]. Also, in another experiment in the temperature range 80K to 200K, c(4×2) was also the dominant component observed [44].

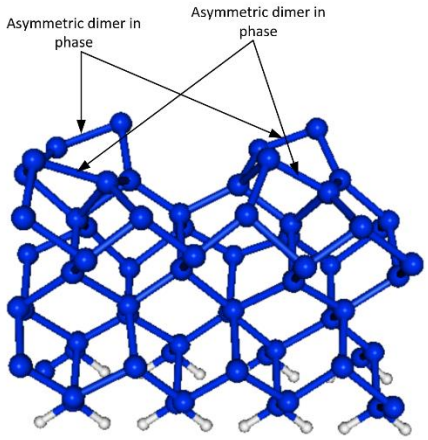

Figure 12. Si(100) p(2x2) surface reconstruction, instantaneous dynamical structure, perspective view. It consists of oriented in parallel dimer rows (two rows are shown), with oppositely buckled dimers along the same row (two dimers are shown in each row), the average simulation temperature is 580K.

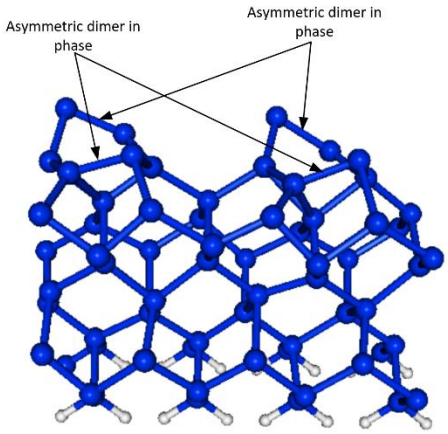

Figure 13. Instantaneous snapshot of Si(100) p(2x2) surface reconstruction, similar to that of Figure 12. The dimers, however, are flipped in both rows relative to Figure 12.

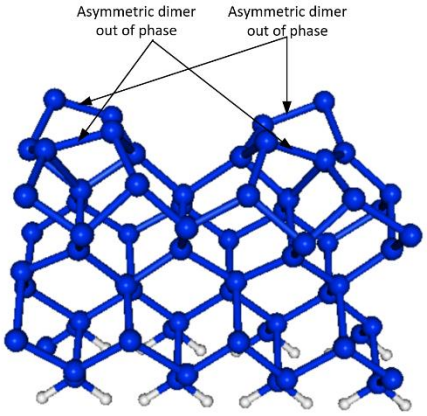

Figure 14. Snapshot of Si(100) c(4x2) surface reconstruction, instantaneous configuration from the 580K average temperature CPMD run, perspective view. It consists of parallel oriented dimer rows (two rows are shown), in a c(4x2) configuration at a temperature of 580K.

Another MD run has been performed at an average temperature of about 300K. The time dependent dimer buckling for this run is shown in *Figure 15*. Even though the figure demonstrates substantial thermal fluctuation of the dimers' vertical shifts, we do not observe the flipping event. It looks like the above finding contradicts the experimental STM results [16]. However, one has to keep in mind that the dimer flipping is a statistical process. Experimentally dimer flipping has been observed at room temperature, but we don't see this in our simulations (see *Figure 15*)

because of the low probability of the dimer flipping occurrence in the MD run, which is due to a short MD run in absolute time. The initial dimer flip, observed at the very beginning of the run, is not considered significant as the system at this point has not sufficiently thermalized from the initial randomized conditions imposed on the geometry. It has been seen theoretically that dimer flipping is more frequent at 900K than 300K [45].

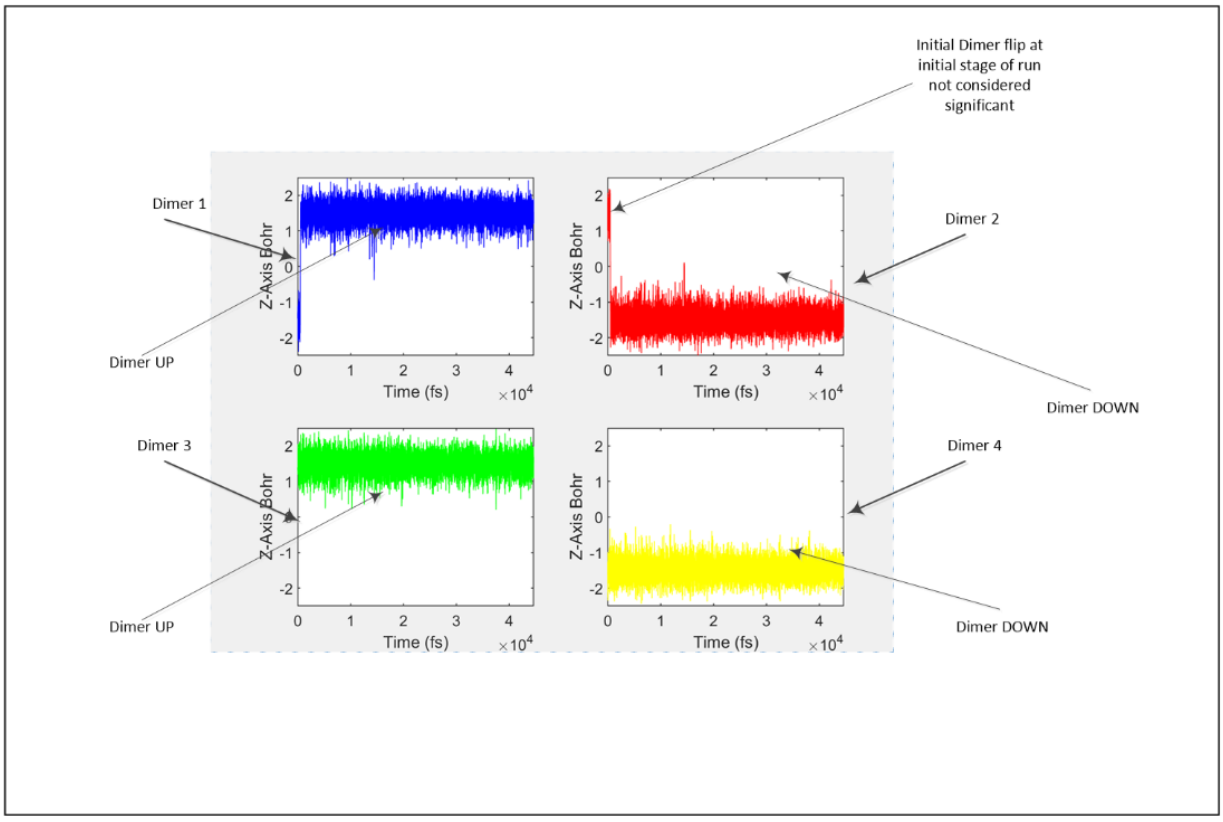

Figure 15. Dimer relative vertical (along Z-axis) displacement on the Si(100) surface, (Units are Bohr), at a temperature of 300K for CPMD. The input Si(100) slab is a temperature of 300K randomized p(2×2) reconstruction. No dimer flipping is observed, i.e., the relative Z-axis height for the dimers does not change as depicted above.

An interesting and unusual result was observed for a CPMD run at a temperature of 600K (see *Figure 16, Figure 17*, and *Figure 18*). While dimers 1 and 2 in the left row demonstrate expected frequent flipping, dimers 3 and 4 from the right row exhibit a symmetric-like configuration. This is seen by the fact that their relative Z-axis height difference fluctuates around zero rather than around positive/negative buckling, as observed in the previous runs.

Also, interesting to note, is that there is experimental observation of a dynamic symmetric like dimer arrangement at 800K [46], which seems to contradict to the previous theoretical and experimental finding. Indeed, it has been shown theoretically by comparing the calculated and the experimental optical responses of clean Si(100), that the asymmetric configurations should dominate at temperatures from 40K to 310K [12]. At higher temperatures the dimer flipping interchanges the microscopic structure between c(4×2) and p(2×2) reconstructions [10], microscopically, however, the dimers are buckled.

In a view of the above theoretical finding of symmetric like dimers, the experimental results of [46] require more investigation, both theoretical and experimental.

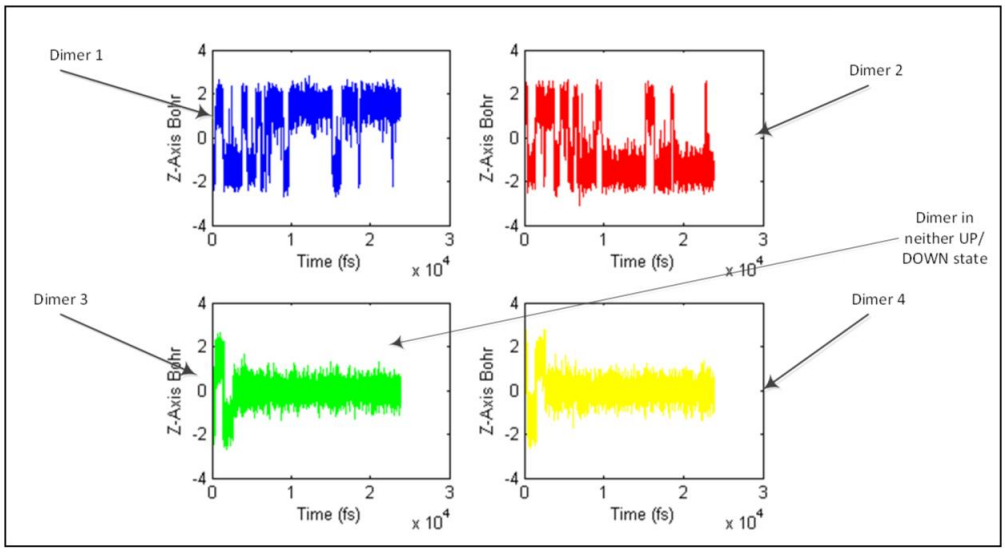

Figure 16. Dimer relative vertical (along Z-axis) displacement on the Si(100) surface, (in Bohr units) at a temperature of 600K for CPMD, input Si slab is at a temperature of 600K with a p(2×2) configuration. All dimers exhibit dimer flipping, i.e., the relative Z-axis height for the dimer flips as depicted above. Two dimers also exhibit a symmetrical configuration, i.e. the average relative Z-axis height is zero (fluctuates around zero).

Theoretically, we attempted to reproduce the effect of symmetric-like dimer behavior by using a larger supercell with CPMD or BOMD as the simulation method. Symmetric dynamical behavior of the dimers, however, was not observed in these simulations.

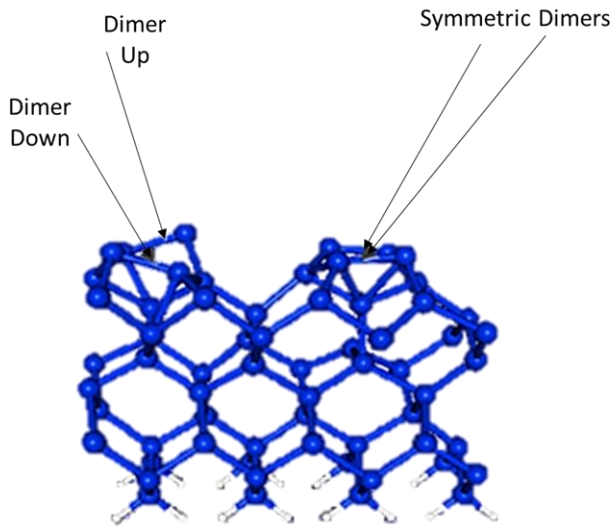

Figure 17. Si(100) surface reconstruction (64 Si atoms), perspective view. Snapshot taken during the CPMD run at a temperature of 600K. Depicts a symmetric-like dimer arrangement, top right of figure and annotated.

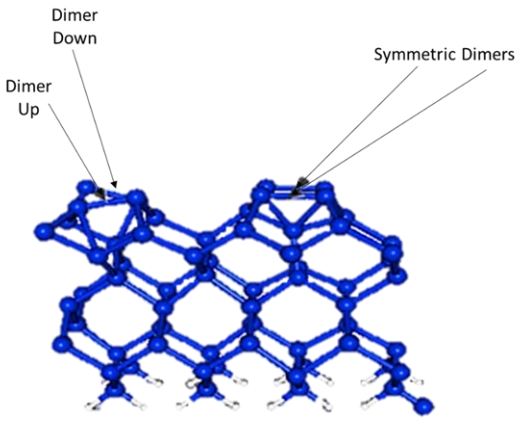

Figure 18. Si(100) surface reconstruction (64 Si atoms), perspective view. Snapshot taken during the CPMD run at a temperature of 600K. The dimers in the left row have flipped from previous figure, while the symmetric – like dimer row (top right of figure and annotated) does not change on average.

Figure 19 shows the results from a molecular dynamics run using the Bohr Oppenheimer MD for simulation at a temperature of 600K, but with two special ***k***-points, which sample the 2D surface BZ in a better way than using Gamma point only. Using the same initial Si(100) slab and its geometry as in CPMD, it is seen that the results are consistent with the Car-Parrinello approach at similar temperatures. However, dynamically stable symmetric-like dimer configurations were

not observed. Further investigations are required to understand the CPMD observed dynamical symmetry of the dimers, shown in *Figure 16*.

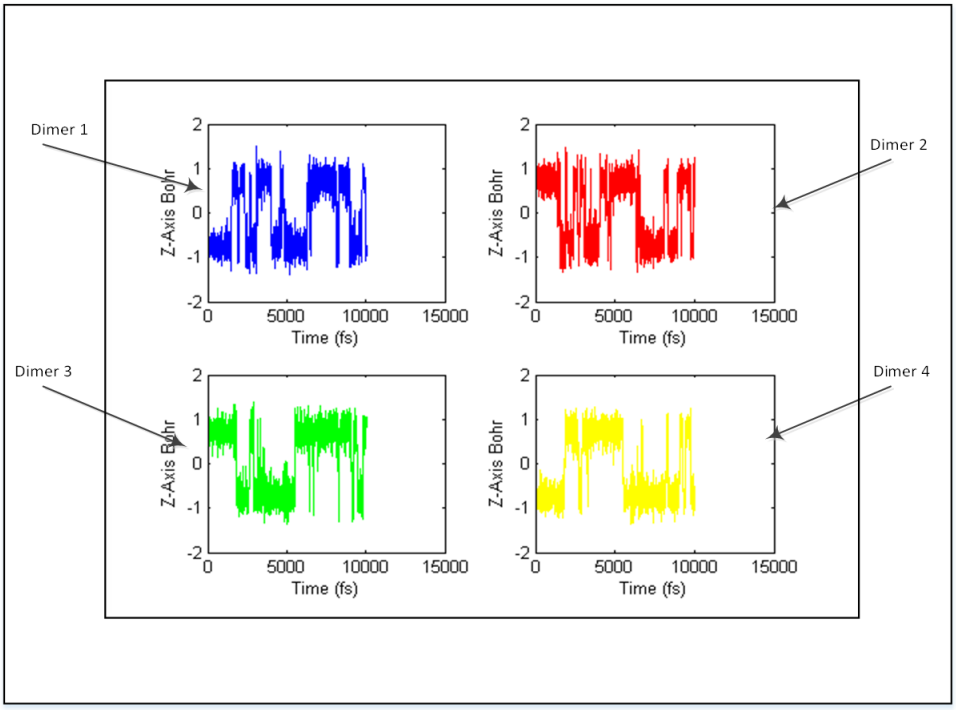

Figure 19. Dimer relative vertical (along Z-axis) displacement from Si(100) Surface using BOMD, the average temperature is 600K. Units are Bohr, the input Si(100) slab has p(2×2) reconstruction. All dimers exhibit dimer flipping, i.e., the relative Z-axis height for the dimer flips as depicted above.

Figure 20 depicts a smaller time scale view of the relative Z-position (100) of the surface Dimer as flipping starts to occur for the BOMD run, shown in *Figure 19.* It is seen that dimers along a row tend to flip simultaneously. This behavior has also been noted in [10]. This flipping can be attributed to the so-called rocking phonon mode of the surface vibrations. There is scope for further study of the dimer rocking mode during a dimer flip by calculating the phonon frequencies using the two different approaches described in the next section.

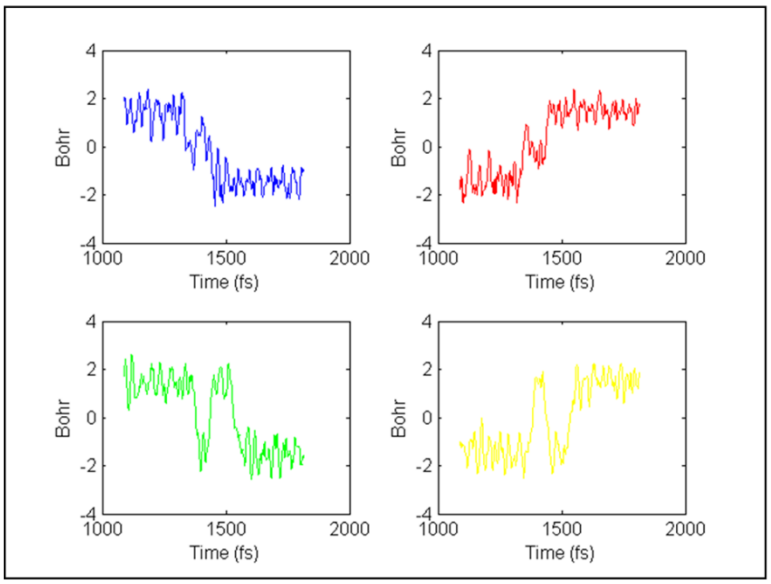

Figure 20. Dimer relative vertical (along Z-axis) displacement from the Si(100) surface, displacement units are in Bohr, the average temperature is 600K for BOMD. The figure has a reduced timescale, compared to Figure 19.

5.1.2 Theoretical Results – Phonon

We calculate the surface atoms vibrational spectra for the clean Si(100) reconstructed surface. Surface vibrational spectra for Si(100) have also been calculated in [10], [25], [47] and confirmed experimentally (see [26] and refs. therein). In contrast to the above cited theoretical papers, we combine and compare the calculated vibrational spectra using two different approaches: (1) the postprocessing of the MD trajectories, which includes anharmonic effects, and (2) the harmonic approach, proposed in [27]. The dimer flipping at the surface, just discussed above, leads to anharmonic terms in the atomic motion. Temperature influences these anharmonic processes, such as atomic structure, electron bands and optical transitions between them.

To account for the dynamical and anharmonic effects, we combine the formalisms of [10,25] to calculate temperature-dependent vibrational spectra of the clean Si(100) surface. Such formalisms do not involve excited electron energy levels, therefore the calculations deal with the ground state properties of the surface. For extracting the phonon frequencies due to the surface vibrations we use two different techniques. The first technique uses density-functional perturbation theory (DFPT) [27], which by principle is harmonic, i.e., it is based on the parabolic approximation when describing the potential energy of the interatomic interactions. In a second

technique we postprocess the temperature dependent MD trajectories through the Fourier transform of the velocity discrete correlation function (the approach is similar to that described in [48]). Since the second method considers real temperature atomic trajectories, it includes anharmonicity implicitly, which should be pronounced when dimer flipping occurs.

Figure 21 depicts the phonon DOS (Density of States) of the Si Bulk (calculated using an input with two Si atoms in the primitive unit cell) and a Si(100) slab with a reconstructed surface (64 Si atoms as used in the previous simulations previously discussed) at a temperature of 0K by applying the harmonic formalism by Baroni [27]. This is also called vibrational DOS, or VDOS.

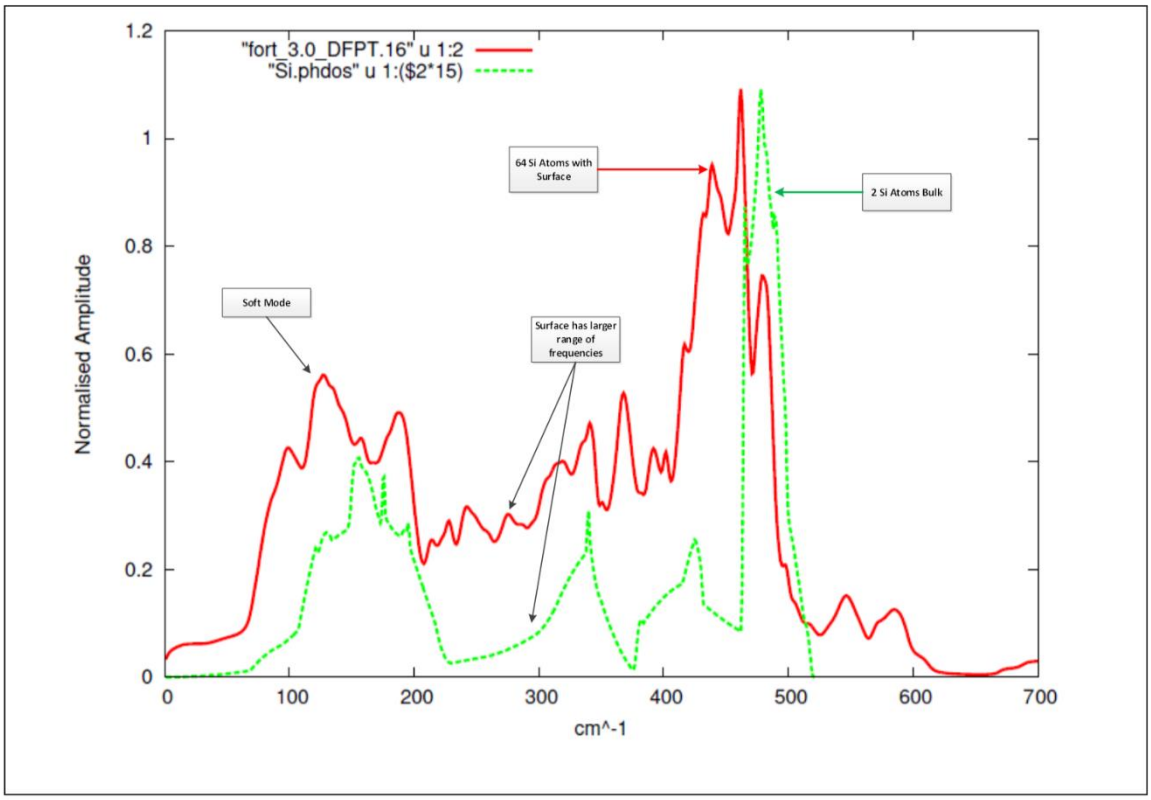

Figure 21. Phonon vibrational DOS for the bulk (two Si atoms) – (green, dashed line) and the ground state, that is at zero temperature) Si(100) p(2×2) reconstruction, calculated for 64 Si atom-slab (red, solid line). The shift to the lower frequency for the zero temperature for the p(2×2) reconstruction (i.e., configuration with a surface, not just the bulk) is expected due to the surface soft phonon mode and surface atoms that are not 4-fold coordinated. The 0K temperature, Si(100) p(2×2) reconstruction does not have the same VDOS minimums as the bulk, due to the surface atoms 3-fold coordination (allowing higher resonant frequencies) and also possible surface structural phase transitions due to dimer flipping.

One has to keep in mind [26] that the relative amplitude between the two curves should not be explained in terms of the vibrational properties of the systems under investigation. The two curves are different due to the difference in the number of atoms in the unit cell used in the model (i.e., the bulk simulation only uses two Si atoms). Therefore, a meaningful comparison can be done mostly in terms of comparing the main phonon frequencies rather than their amplitudes.

The vibrational response of the (100) surface slab does not demonstrate the same minimums in VDOS that the bulk has. Several reasons can be considered to explain this effect. In the Si bulk each atom has 4 neighbors (that is 4-fold coordinated), but on the surface, the dimer atoms are 3-fold coordinated, which results in a larger variety of atomic motion, which should result in more resonant frequencies. Conversely, a lower coordination number should also lead to lower vibration frequencies. Furthermore, observation of abnormally low frequencies (the so-called soft phonon modes) in both experiment and theory, indicates a possibility of surface structural phase transitions. For the Si(100) surface this is actually a c(4×2) ↔ p(2×1) order-disorder phase transition. This has been confirmed by experiment [26]. On the other hand, structure determination using LEED, consists of fitting the experimental pattern with different structures. Despite an apparent 2×1 LEED pattern, the fit matches c(4x2) or p(2x2) structures.

In *Figure 21* we actually demonstrate substantial modification of the bulk modes due to the presence of the (100) surface. However, the slab is eight layers in the model, but in reality there will be many more bulk layers relative to the surface. Therefore in the model's case the surface contribution is accentuated to what it would be in experiment.

Appearance of the higher vibrational frequencies for the Si(100) reconstructed surface requires more investigation. The atoms that have these frequencies would need to be identified, which is included in the future work section. A possible reason of the frequency increase can be that some atom bonds close to the surface might be compressed due to the dimerization, and demonstrate a higher frequency (shorter wavelength) than in the bulk. Their bonds might be compressed which add the higher frequency component to the VDOS. Although there are no recent studies of the phonon spectra of Si(100) surface, the helium scattering experiment, carried out in a wide range of temperatures at the clean Ge(100) [49], which is structurally and dynamically very similar to Si(100), indicates the phonon frequency modification effect we observe in our simulations.

The red frequency shift for the surface slab reconstruction is expected due to the surface soft phonon mode and surface atoms that are not 4-coordinated.

Figure 22 depicts the Si(100) VDOS, calculated using the Velocity Auto Correlation technique (i.e., postprocessing of temperature dependent MD trajectories through the Fourier transform of the velocity discrete correlation function) on the Si(100) slab after CPMD (Car Parrinello Molecular Dynamics) have been used to produce these trajectories. This method includes anharmonicity implicitly. Two sets of dynamical trajectories for Si(100) slabs at two different temperatures of 300K and 600K have been postprocessed. We recall that no dimer flipping has been observed at a temperature of 300K , while the dimers flip frequently at 600K.

From the MD results we observe that dimers from different rows flip independently. This is also due to the fact that the two high order Si(100) reconstructions are practically degenerate in energy. Within the row, dimer flipping is strongly correlated in such a way that the neighboring dimers are always oppositely oriented.

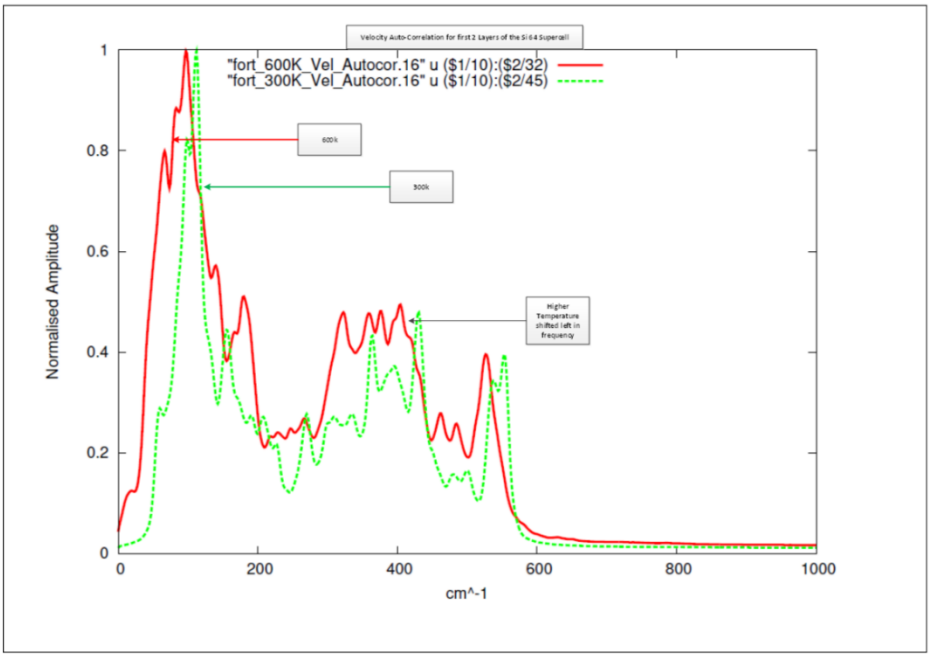

Figure 22. Surface phonon spectra using the Velocity Auto Correlation formalism on dynamical output from two different temperature CPMD runs. Molecular trajectories (Si(100) slab surface layer) from CPMD runs at temperatures of 300K (green line, dashed) and 600K (red line) were used as input to the Velocity Autocorrelation Program. It is seen that the higher temperature CPMD run at 600K (red line) is shifted to lower frequency relative to the lower temperature 300K CPMD run (green line). This is a known effect from experiment [49].

With anharmonic terms now included, higher frequency contribution to VDOS can be seen. The origin of this high frequency contribution requires further investigation. Using Velocity Autocorrelation, it is possible to pick atoms in different layers to try to identify modes of vibration. This can be considered for the future work.

The temperature dependent red VDOS shift at higher temperatures is demonstrated, which is clearly the result of anharmonicity. This has been observed and is a known effect from experiment. [26].

5.1.3 Theoretical Results – Optical Response

The surface optical response, more formally termed temperature dependent reflectance anisotropy (RA), was calculated for several molecular dynamics runs that correspond to different temperatures (from 300K to 600K) as well as for the ground states of the Si(100) surface, that is at zero temperature. RA spectroscopy (RAS) is based on the fact that the surface linear optical response is anisotropic, while for the bulk of cubic semiconductors it is isotropic, therefore a difference in the linear response along two main Si(100) directions should be only surface related. While all the previous calculations of the Si(100) surface RA have been done for 0K structures, [61]and refs. therein, and [41]), our goal is to prove that the high temperature optical response can be also calculated with the main experimentally observed features reproduced. For this the finite temperature Car-Parrinello Molecular Dynamics (CPMD) runs were carried out at a temperature of 300K and 600K to provide temperature-dependent atomic structural input. When calculating the optical response at nonzero temperature, the dynamical contribution to the optical response was included through averaging the optical responses for several representative temperature-perturbed atomic configurations (atomic snapshots). In this simulation we follow the theoretical formalism, developed and applied to GaAs and Si bulk semiconductors in [38], [42], shown to be in agreement with the experimental results, namely a temperature-induced shift of both surface and bulk optical peak to lower energy and broadening, which we reproduced in the model.

The temperature induced modification of the optical response should be substantially more pronounced for the surface atoms than for the Si bulk atoms due to dynamical peculiarities of the dimer motion [10]. However, usually the RA is measured at room temperature and calculated for the 0K (ground state structure) [41], as demonstrated in *Figure 23* below.

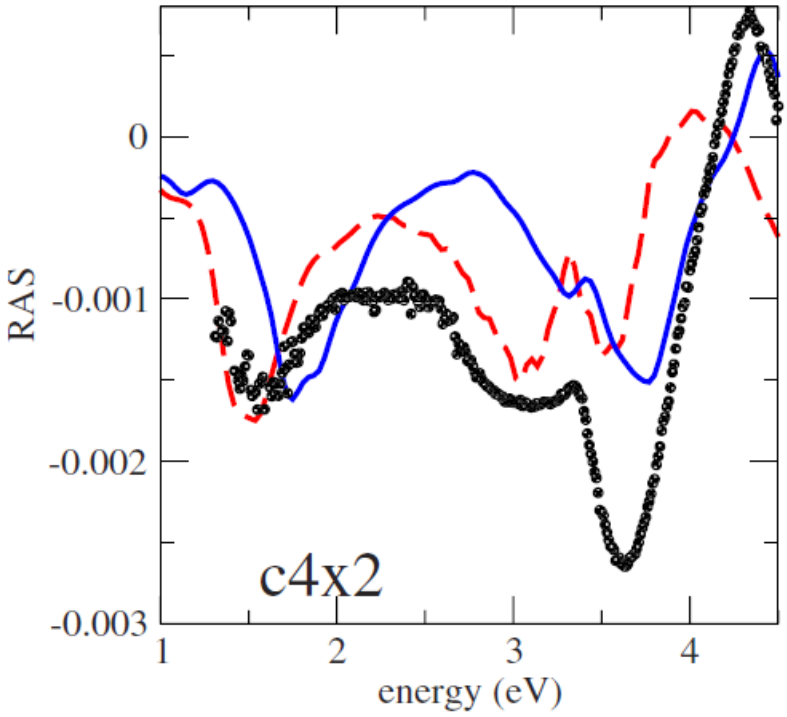

Figure 23. Measured at a temperature of 300K Si(100) surface RA (dots) and DFT-LDA (i.e. calculated) at 0K (red dashes), DFT – LDA with scissor shift (blue solid), reflectance anisotropy (RA) for c(4×2) reconstruction [41].

To the best of our knowledge, the temperature dependent RA measurements at the clean Si(100) surface have only been done in Prof. Y. Borensztein group ([56], private communication). In their experiment the temperature range was 300K – 1283K, the reflectance anisotropy was measured between 2 and 5 eV. (*Figure 24*). You can see from *Figure 24* (i) the fast disappearance of the 1.6 eV transition peak (it actually shifts to the lower energy, which is outside the spectrometer range), and (ii) the red shift of the main RA peaks, followed by damping of the feature at 3.1 eV; the red shift and the damping of the bulk feature at 3.6/4.35 eV.

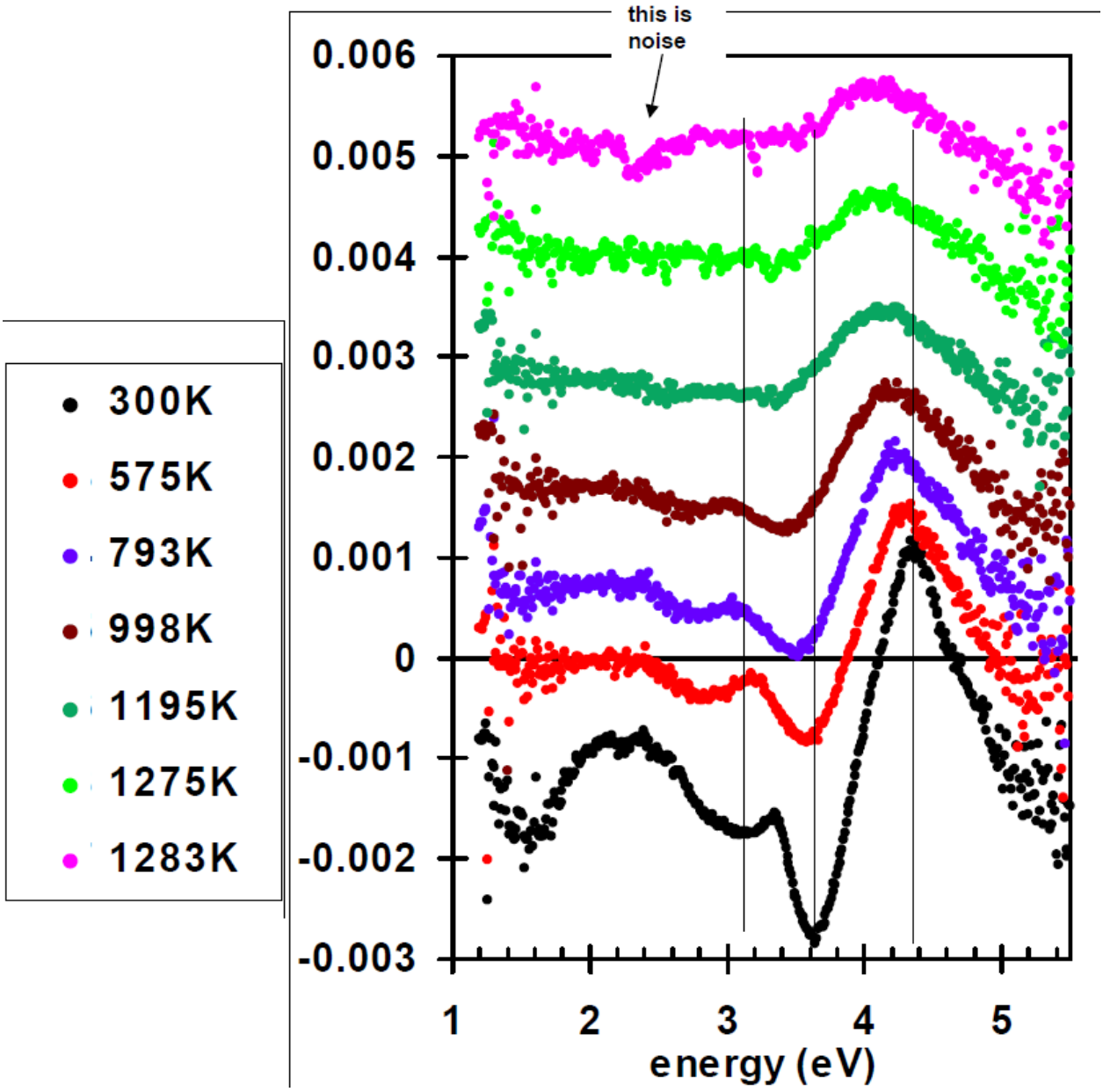

Figure 24. Temperature dependent RA of the clean Si(100) surface, measured in the temperature range 300K – 1283K [56].

To prove that the above experimental features can be theoretically reproduced, we calculated the RA for Si(100) surface at the MD temperature of 600K. For this temperature we see that all the temperature dependent experimental features can be successfully modelled in the calculated RA.

The following figures show results of the calculation of the temperature dependent reflectance anisotropy (RA).

The Quantum Espresso Epsilon Procedure calculates the Linear Optical Response, namely the dielectric function, along three main directions. As a Si 3d crystal is optically isotropic the dielectric function is spatially isotropic, it becomes, however, anisotropic for the Si(100) surface.

We calculate first the optical response of the Si bulk (using the primitive unit cell with two Si atoms) and next the optical response of the Si(100) surface using the 64 Si atom supercell at 0K for the p(2×2) and c(4×2) reconstructions. For the surface optical calculation a homogeneous 32 × 32 grid of 1024 ***k***-point has been used. After that the dielectric function of the clean Si(100) surface at 600K was calculated.

For the 0K temperature p(2×2) and c(4×2) reconstructions we calculate the RA for both configurations by taking the optical response difference between the X and Y directions. This corresponds to a RAS experiment with normal incidence to the surface. As the bulk is optically isotropic, any difference in the optical response between the X and Y directions would be due to surface induced effects.

Next we calculate the RA for Si(100) at the 600K temperature c(4×2) configuration. This was carried out by taking four representative snapshots of the 64 Si supercell from a CPMD run at an average temperature of 600K, calculating RA for each snapshot and then taking the average of the linear optical response of the four snapshots.

We now will analyze the differences between the optics of the ground state and temperature perturbed surface, as shown in next five figures. We note that all these figures except the last *Figure 30* have been postprocessed with Gaussian smoothing.

Figure 25 depicts the frequency dependence of the linear optical response for the Si bulk, as well as the response for the p(2×2) and c(4×2) reconstructions at zero temperature.

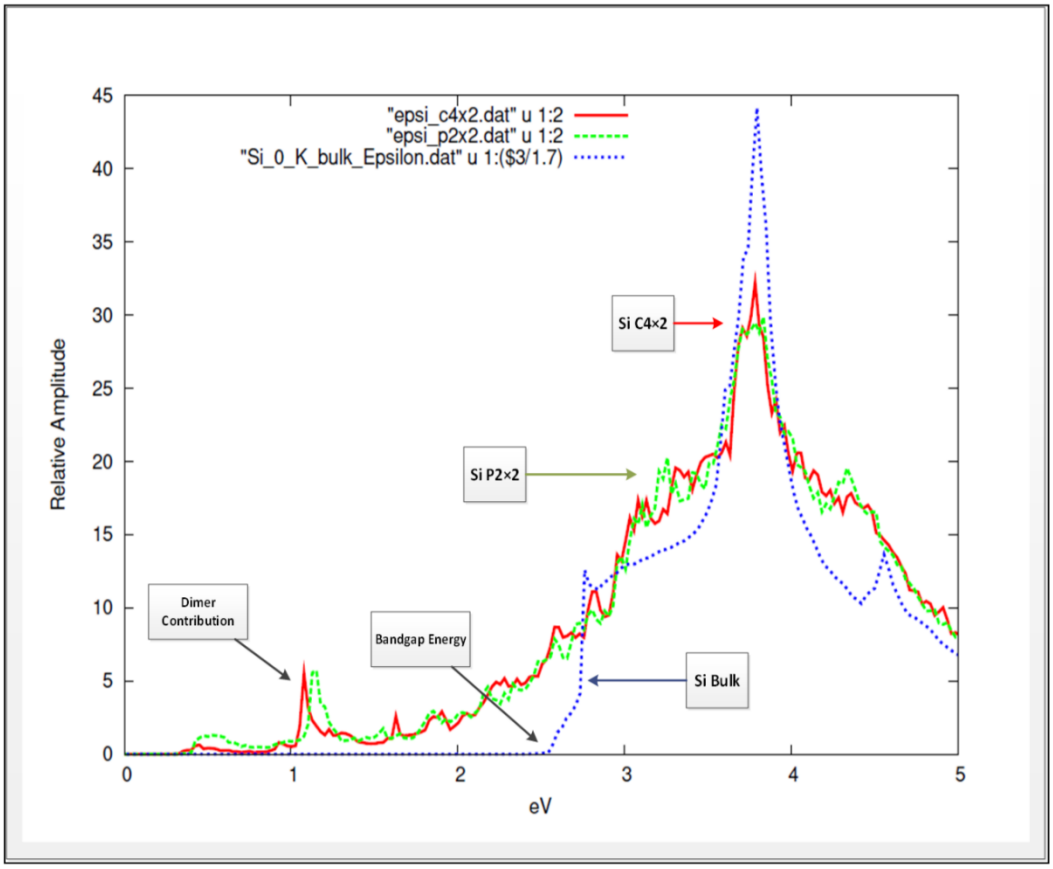

Figure 25. Linear Optical Response at 0K temperature for Si(100) p(2×2)-(green line, dash) and c(4×2)-(red line, solid) reconstructions (using a 64 Si atom slab) and the Si bulk dielectric function-(blue line, dotted)-(with two Si atoms). The optical bandgap energy for the bulk (blue line) can be seen at 2.6eV (we do not apply the scissors corrections), and surface dimer contributions start at 1.2eV. Direct dimer related optical transitions appear at 0.5eV.

The position of the main bulk peak for the imaginary part of the dielectric constant is 3.7eV (8.7 × 10^{14} Hz) which is in good agreement with the theory of [50]. The optical response peaks for the two surface configurations p(2×2) and c(4×2) are also at the same energy, 3.7eV (8.7 × 10^{14} Hz). This optical response peak for the p(2×2) and c(4×2) reconstructions will also include contributions from the bulk.

The optical bandgap for the bulk at 2.6eV is less than experiment, where 3eV is measured [51]. This reflects a well-known limitation of the optical calculations using the DFT - LDA approximation. Optical absorption corresponds to a direct bandgap transition at the same ***k***-point between the filled and empty states (the so-called vertical transitions).

The lowest energy of the direct transition (same ***k***-point) is 0.5eV for the c(4×2) reconstruction, with the p(2×2) reconstruction having a just slightly higher (additional 0.1 eV) energy, for this transition. This transition for both reconstructions is due to surface contributions, i.e., it does not occur for the bulk as seen in *Figure 25*.

Contributions to the optical absorption are also seen at 1.2eV, they can be attributed to the Si(100) surface dimers.

Figure 26, *Figure 27* and *Figure 28* show the surface contribution to the dielectric function of three configurations, 0K temperature, c(4×2), 0K temperature, p(2×2) and 600K temperature, c(4×2). Each figure also shows the RA, calculated by taking the optical response difference between the X and Y directions for each reconstruction (i.e., in the plane of the surface).

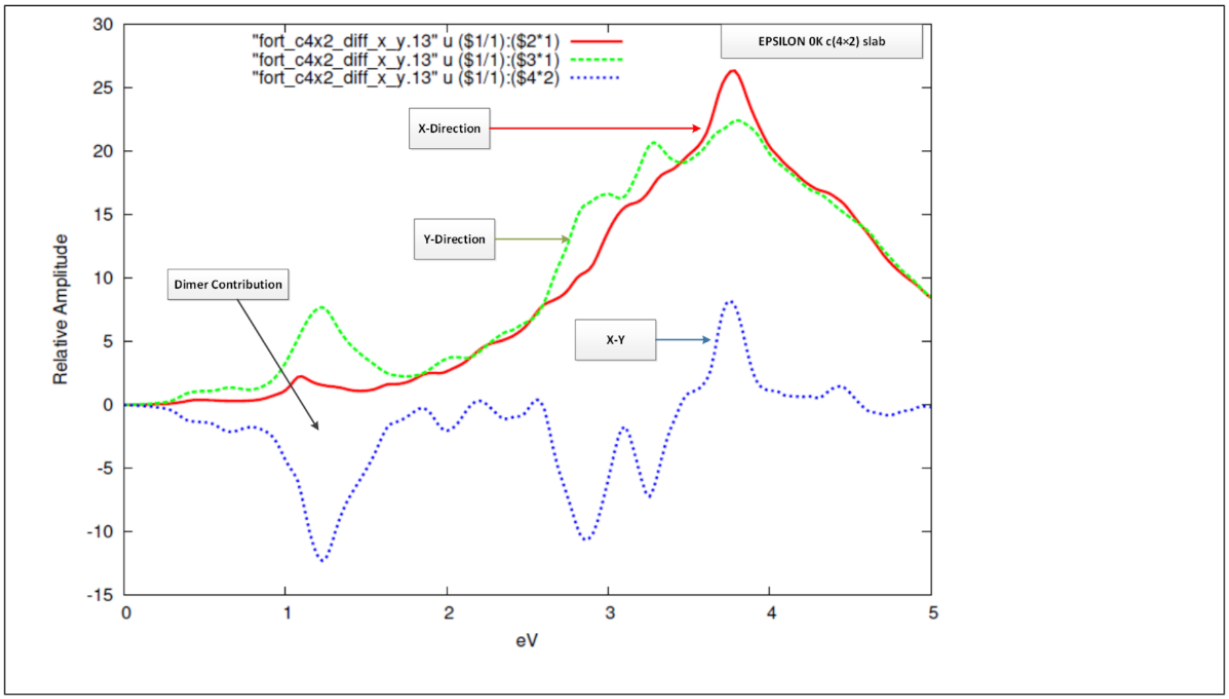

Figure 26. Reflectance anisotropy (optical response difference between the X and Y direction, X-Y)- (blue line, dotted) at 0K for Si(100) c(4×2), and Linear Optical Response in the X –direction (red line, solid), and Y -direction (green line, dash) for Si(100) c(4×2) reconstruction at 0K temperature. Surface dimer absorption is seen at 1.2eV, and at 3.7eV.

In *Figure 26* the peak at 1.2eV for the RA (blue line, dotted) is due to surface dimer contribution. A peak on the same line can be seen at 3.7eV, which is at the same energy as the bulk absorption peak shown in *Figure 25*.

In the same *Figure 26*, there are also two peaks either side of 3eV at 2.8eV and 3.3eV respectively, that indicate surface absorption for these two energies. The 0K temperature p(2×2) reconstruction shown in the next *Figure 27* does not exhibit the same absorption at these energies.

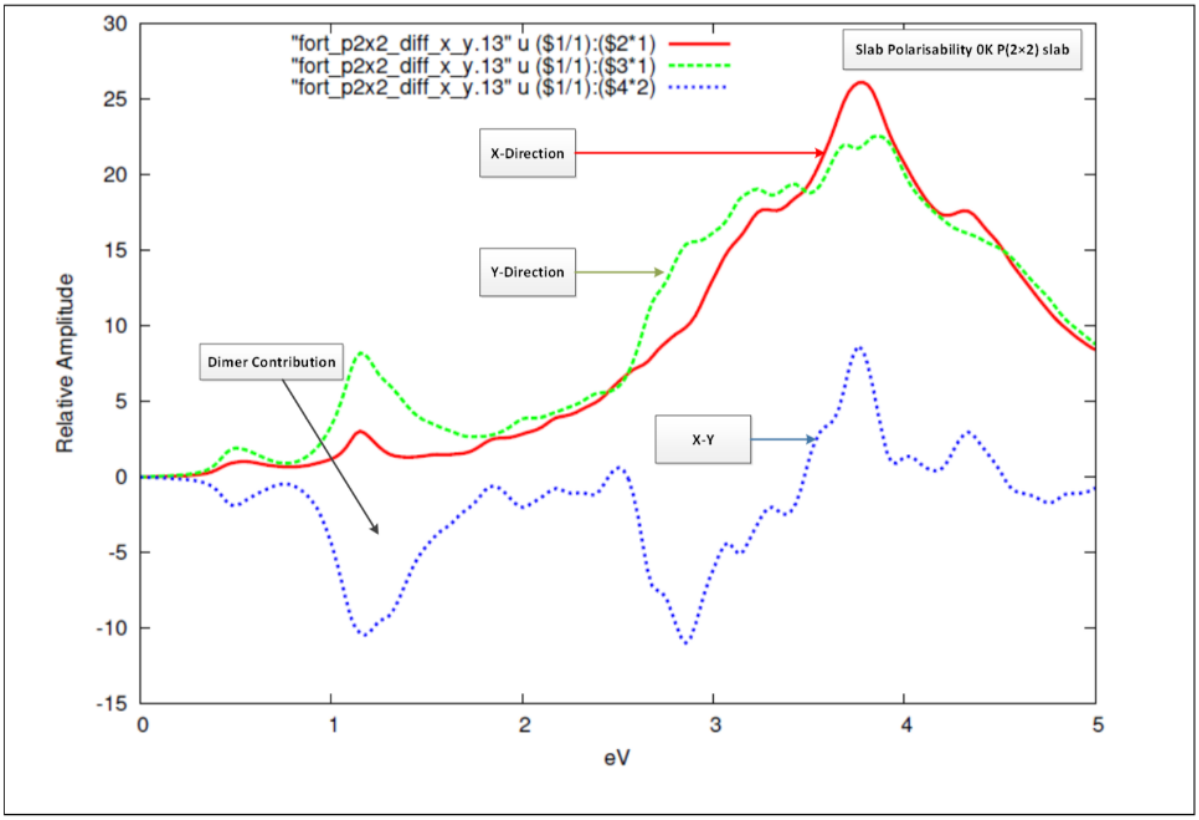

Figure 27. Reflectance anisotropy (optical response difference between the X and Y direction, X-Y)- (blue line, dotted) at 0K temperature for Si(100) p(2×2), and linear optical response in the X – direction (red line, solid), and Y -direction (green line, dash) for Si(100) p(2×2) reconstruction at 0K temperature. Surface dimer absorption is seen at 1.2eV, and at 3.7eV.

The RA in *Figure 27* (blue line, dotted) is similar to the 0K temperature, c(4×2) reconstructed slab response in *Figure 26*, with the peaks for RA at 1.2eV and 3.7eV.

However, in *Figure 27* the peak at 3.3eV observed for the c(4×2) reconstruction in *Figure 26* is not present.

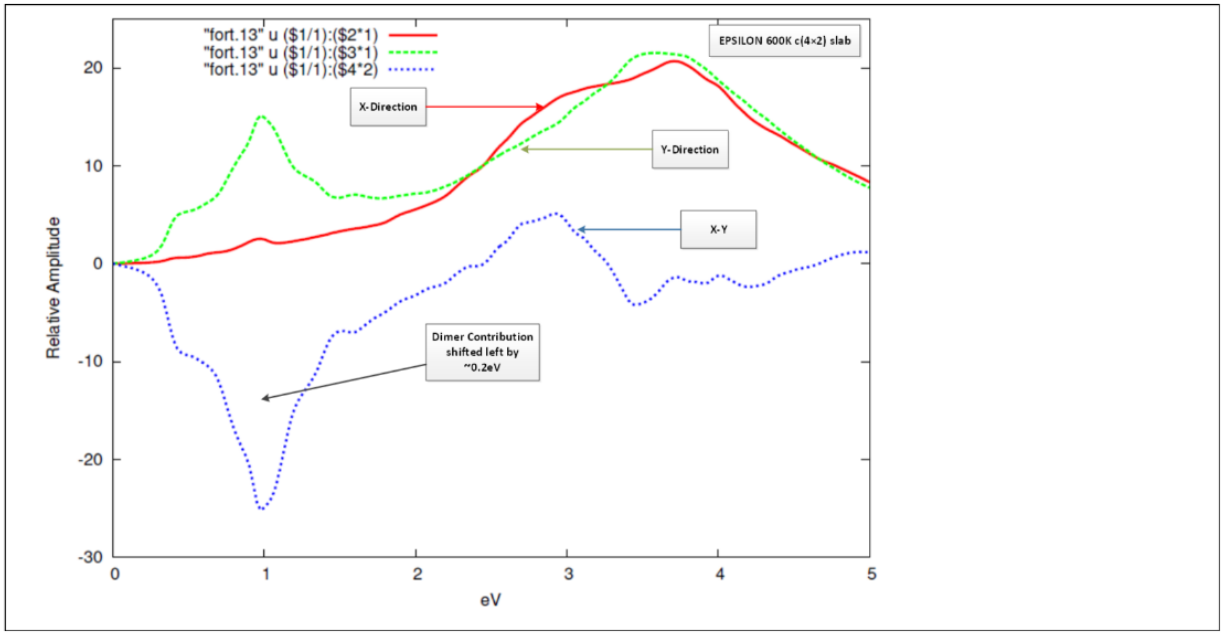

Figure 28. Reflectance anisotropy (optical response difference between the X and Y direction, X-Y)- (blue line, dotted) at a temperature of 600K for Si(100) c(4×2), and optical response in the X – direction (red line, solid), and Y -direction (green line, dash) for Si(100) c(4×2) at a temperature of 600K. The surface dimer absorption is seen shifted to 1eV and 3eV from 1.2eV and 3.7eV from the previous two figures for the 0K temperature reconstructions.

Figure 28 depicts the RA with a Si(100) c(4×2) configuration at a temperature of 600K (four snapshots taken from a 600K average temperature CPMD run, with the Optical Response averaged over the four snapshots). The surface dimer contribution seen at 1.2eV for the 0K temperature reconstructions for the RA (blue line, dotted), *Figure [26,27],* is shifted left by approximately 0.2eV. The contribution of the surface dimer to the RA difference between the X and Y direction is also higher than the reconstructions at 0K temperature, *Figure [26,27].* The peak seen at 3.7eV for the 0K temperature reconstructions *Figure [26,27],* is shifted to 3eV in *Figure 28.*

The shift in the surface dimer contribution to the RA (optical response difference between the X and Y direction) with the temperature increase has been actually observed experimentally. [56]

Figure 29 below shows the comparison between the experimental results presented in Figure 24 and our results in Figure 26, 28.

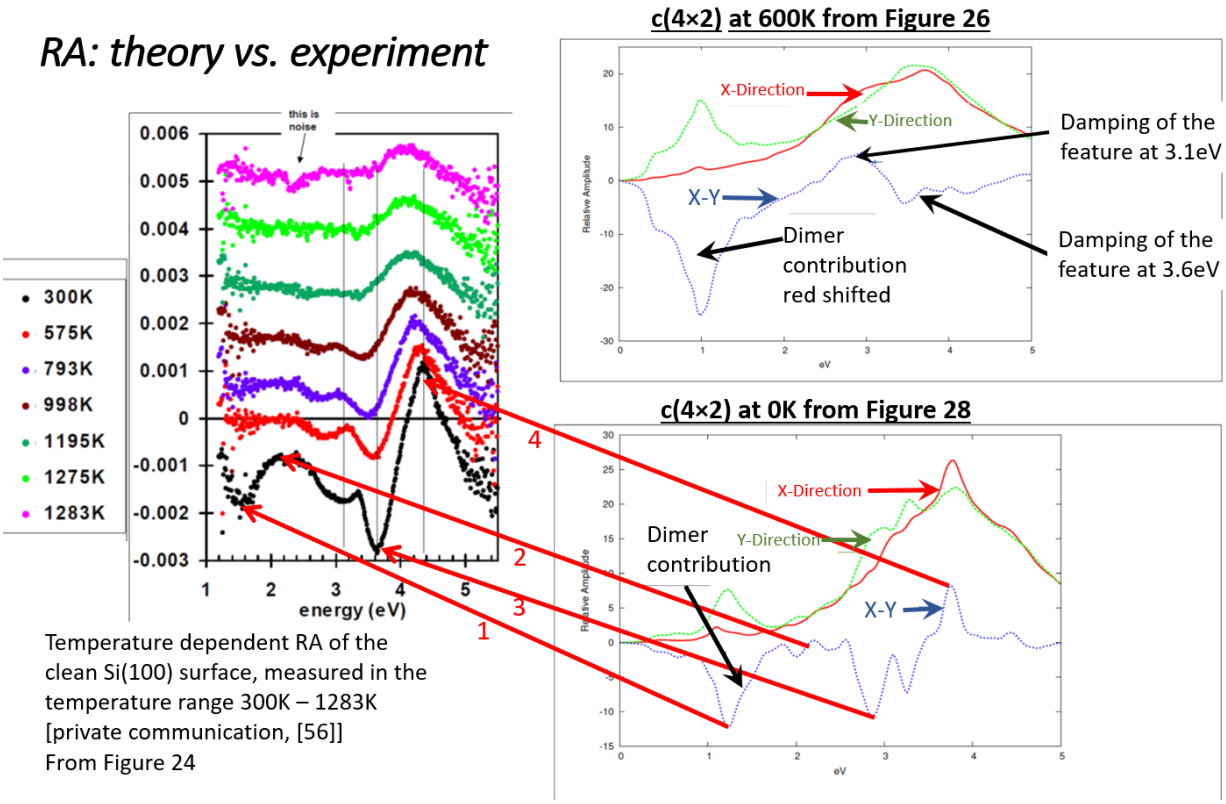

Figure 29. A comparison between Figure 24 (experimental results) and our results in Figure 26, 28. The red arrows from Figure 28 to Figure 24 identify the similar features in our model to experiment (in this case the 300k experimental result). Arrow (1) identifies the dimer induced peak at 1.6eV in the experiment, arrow (2) the peak at 2.2eV, arrow (3) the peak at 3.6eV and arrow (4) the peak at 4.4eV. As the temperature increases we can also see in Figure 26 (at 600K) a red shift that also occurs in experiment, Figure 24 at 575K (red line), and a damping of the peaks observed at the lower temperature (0K in our model) and in experiment.

It should be noted that the LDA approximation used in our model (DFT) will cause the actual energies to be less than those observed in experiment, this is a known feature of the LDA approximation.

In Figure 29, it can be seen that once the energy shift left due to the LDA approximation is noted, there is a good agreement between the model in Figure 28 RA, and the experimental results in Figure 24,at 300K, indicated by the red arrows in Figure 29.

As we move to a higher temperature of 600K in our model, Figure 26, we also see the broadening/damping of the peaks that are also seen in Figure 24, as the temperature increases to 575K.

Furthermore the red shift of the peaks, and the dimer contribution peak at 1.6ev, as the temperature is increased, shown in the experimental results in Figure 24, are observed in our model at 600K in Figure 26. As mentioned previously, in the experimental results in Figure 24, the dimer induced peak at 1.6eV is red shifted out of the measuring range of the experimental equipment, and this is why it disappears into noise with higher temperatures in the experimental results presented.

We also calculate electronic density of states (DOS) for the Si reconstructions (64 Si atoms) under consideration. The DOS is the number of available states at each energy per unit volume. It can be used to identify band gaps in semiconductors and other significant energy levels which can be matched with experiment.

The Quantum Espresso software package was used to calculate the electronic Density of States (DOS), with the specific Si reconstruction used as input. In this case the Si bulk (two Si atoms), and the 0K temperature, p(2×2), c(4×2) reconstructions (64 Si atoms) as used in the linear optical response calculations of the previous section, were used to calculate the DOS. See *Figure 29*.

We also calculated the DOS for the 300K and 600K temperature Si configurations, taken as snapshots from CPMD runs at those average temperatures. In this case three p(2×2) supercell snapshots were taken from the 300K temperature, CPMD run, and four c(4×2) supercell snapshots from the 600K temperature, CPMD run, to be used as inputs to the DOS calculation. The average DOS result was then taken for the snapshots for each temperature. See *Figure 30.*

Figure [29, 30] show the Density of States in the optical frequency range of reconstructions at 0K, 300K and 600K temperatures.

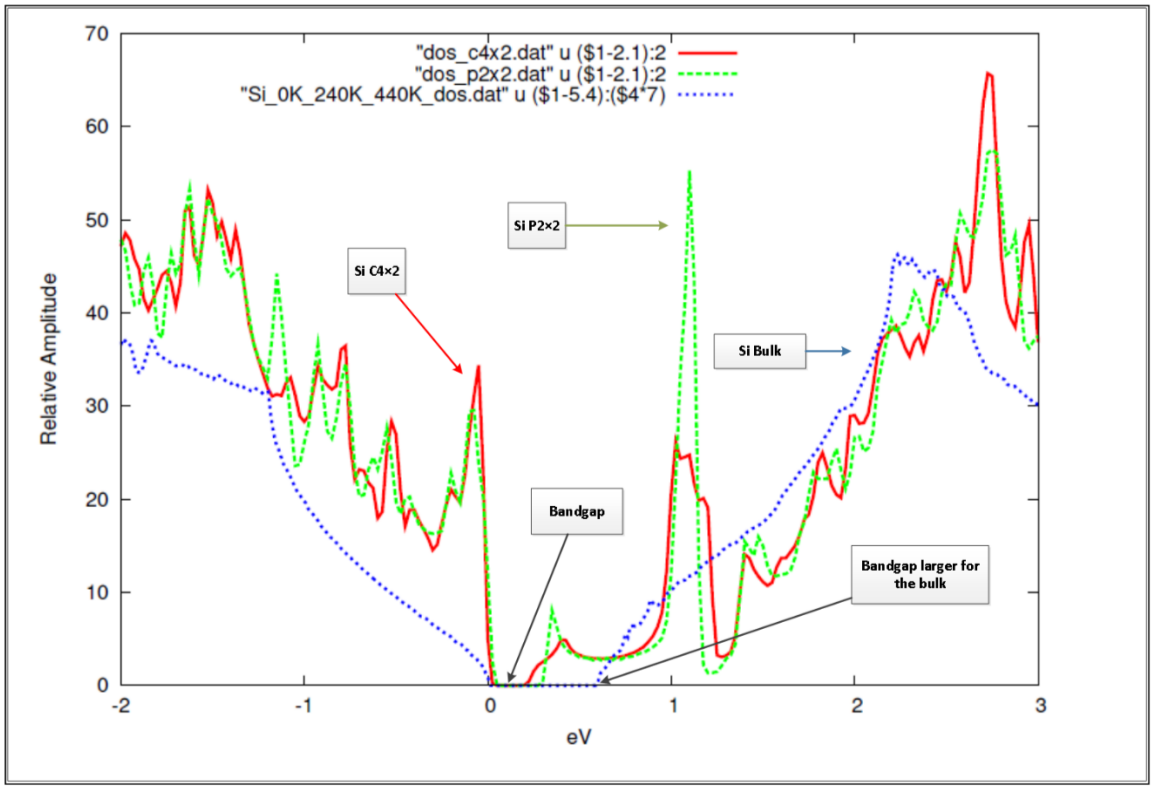

Figure 30. Band gap electronic DOS at 0K temperature, calculated for Si(100) p(2×2) reconstruction (green line, dash), c(4×2) reconstruction (red line, solid) and bulk (two Si atoms) (blue line, dotted). The bandgap for the three configurations has been aligned to start at 0eV, with negative energy corresponding to filled states below the bandgap and states above the bandgap with positive energy. It can be seen that the bandgap from DOS is larger for the bulk (blue line) compared to the reconstructed Si(100) surface.

In *Figure 30*, the negative energies represent the filled states below the bandgap, and positive energies the states above the bandgap.

The DOS for Si bulk demonstrates the larger bandgap (since there are no contributions from the surface states). The DOS for the p(2x2) and c(4x2) reconstructions have bandgaps which are close in value, of 0.3eV and 0.25eV respectively, but reduced in comparison to the bulk which has a bandgap of 0.6eV.

Theoretically it is expected that the surface contributions will reduce the bandgap as the bonds on the surface are weaker relative to the bulk bonds, which results in a reduction of the absorption energy required for a bandgap transition [9]. Also there is termination in the Z-direction (normal to the surface), which generates the surface states [52].

In *Figure 31* we plot the DOS of two configurations both taken as snapshots from a CPMD run, one at a temperature of 300K and the other at 600K.

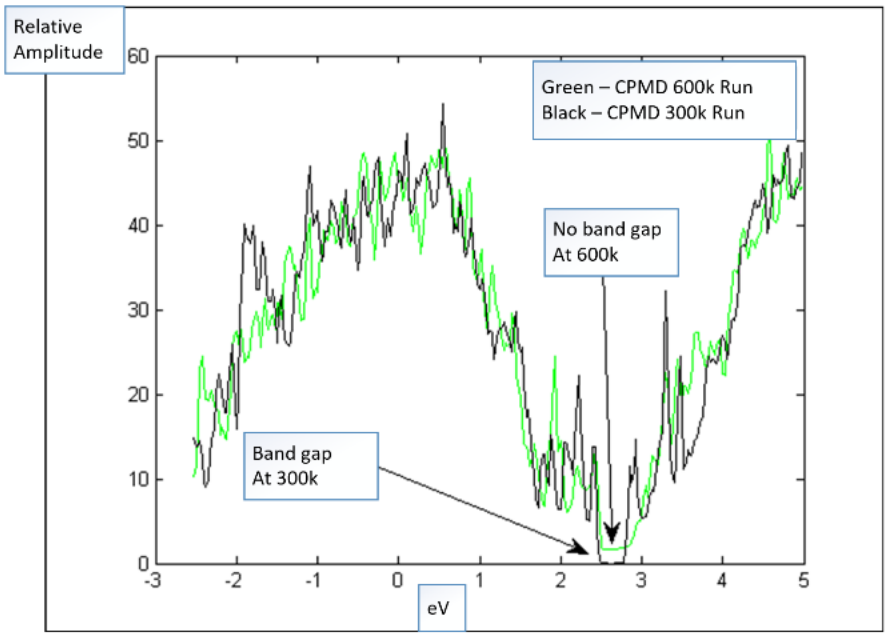

Figure 31. DOS for Si p(2x2) at a temperature of 300K (black line) and Si c(4x2) at a temperature of 600K (green line) Si configurations, taken as snapshots from the dynamical output of CPMD runs at temperatures of 300K and 600K respectively. This graph has not been smoothed or shifted to 0eV for where the bandgap starts, as in the previous figure. This postprocessing has not been done for this graph in order to show that at 600K the bandgap disappears as annotated in this figure.

In *Figure 31* at a temperature of 300K the bandgap is narrowed compared to the 0K temperature reconstructions shown in *Figure 29*. As the system's temperature increases, the interatomic distances oscillate around the equilibrium distance at 0K temperature, and this reduces the bandgap. This effect is known from theory: the most stable structure demonstrates the largest gap. The theory shows that if the bond length is either increased or decreased from the 0K equilibrium length, the bandgap decreases [38].

5.1.4 Results Summary in Table Format

A summary of all the results in tabular format is given below.in *Table 4.*

Figure	**Temp (K)**	**Calculation Type**	**Result Highlights**	**Number of steps, Length of step (fs), Total Time (fs)**	**Average Dimer Length**	**Average Dimer Height (Bohr units)** Note: 1 = Dimer 1 2 = Dimer 2 3 – Dimer 3 4 = Dimer 4 **<u>Above</u> = relative dimer Z-axis height is > 0 and <u>Below</u> = relative dimer Z-axis height is < 0 See explanatory note below table**	**Ground State Dimer Length** Note: 1 = Dimer 1 2 = Dimer 2 3 – Dimer 3 4 = Dimer 4
Fig 11	580K	CPMD	1. Dimer flipping observed	14804, 0.120944, 1.7905e+03	1. 2.4014 2. 2.3982 3. 2.3987 4. 2.3986	Above (Z>0): 1. 1.3848 2. 1.4542 3. 1.3909 4. 1.3961 Below (Z<0): 1. -1.3915 2. -1.3266 3. -1.3895 4. -1.3517	1.2.1937 2.2.3534 3.2.3534 4.2.3536
Fig 15	300K	CPMD	1. No dimer flipping observed	368992, 0.120944, 4.4627e+04	1. 2.3942 2. 2.3940 3. 2.3941 4. 2.3941	Above: 1. 1.4834 2. 1.3887 3. 1.4875 4. n/a Below: 1. -1.3510 2. -1.4796 3.n/a 4. -1.4829	1.2.1937 2.2.3534 3.2.3534 4.2.3536
Fig 16	600K	CPMD <u>Input:</u> 0K p(2×2) Si slab	1. Dimer flipping observed 2. Symmetric dimers observed	196979, 0.120944, 2.3823e+04	1. 2.3970 2. 2.3993 3. 2.3999 4. 2.4256	Above: 1. 1.4245 2. 1.3417 3 0.4119. 4. 0.4473 Below: 1. -1.3424 2. -1.4166 3. -0.4359 4. -0.4275	1.2.1937 2.2.3534 3.2.3534 4.2.3536

Fig 19	600K	BOMD <u>Input:</u> 0K p(2×2) Si slab	1. Dimer flipping observed 2. No symmetric dimers observed	83060, 0.120944, 1.0046e+04	1. 2.5105 2. 2.5113 3. 2.5087 4. 2.5121	Above: 1. 0.6701 2. 0.8321 3. 0.9167 4. 0.6244 Below: 1. -0.6941 2. -0.5541 3. -0.4768 4. -0.7649	1.2.1937 2.2.3534 3.2.3534 4.2.3536
Fig 21 (Phonon Response vs Frequency)	0K	DFPT <u>Input:</u> a. p(2×2) slab b. Si bulk	1. Red shift in frequencies for the surface observed 2. Difference in vibrational minimums for the surface	n/a	n/a	n/a	1. 2.3544 2. 2.3542 3. 2.3542 4. 2.3544
Fig 22 (Phonon Response - anharmonic)	a. 300K b. 600K	Velocity Auto Correlation <u>Input:</u> a. Si slab surface atomic layer dynamical output from CPMD 300K run b. Si slab surface atomic layer dynamical output from CPMD 600K run	1. Red shift in the frequencies for the higher temperature.	n/a	n/a	n/a	n/a
Fig 25 (Linear Optical Response)	0K	Linear Optical Response <u>Input:</u> a. 0K p(2×2) slab b. 0K c(4×2) slab c. Si bulk (2 Si atoms)	1. Main peak at 3.7eV in agreement with theory. 2. Bandgap for bulk less than experiment due to LDA Approximation. 3. Surface direct transitions at 0.5eV.	n/a	n/a	n/a	<u>0K p(2×2) slab</u> 1. 2.3569 2. 2.3535 3. 2.3548 4. 2.35565 <u>0K c(4×2) slab</u> 1. 2.3557 2. 2.3568 3. 2.3568 4. 2.3566
Fig 26 (RA)	0K	RA, obtained by subtracting Y Axis Optical Linear Response from X-Axis Optical Linear Response. <u>Input:</u> 0K c(4×2) slab	1. Surface dimer contribution at 1.2eV, and main peak at 3.7eV similar to the bulk.	n/a	n/a	n/a	n/a

Fig 27 (RA)	0K	RA. <u>Input:</u> 0K p(2×2) slab	1. Similar to 0K c(4×2) slab in above figure.	n/a	n/a	n/a	n/a
Fig 28 (RA)	600K	RA (averaged over four RA from the four Si slabs used as input) <u>Input:</u> Four c(4×2) slabs taken as four slab snapshots from the dynamical output of a 600K CPMD run	1. RA response shifted left due to higher Temperature	n/a	n/a	n/a	n/a
Fig 30 (Electronic Density of States)	0K	DFT to calculate Electronic DOS. <u>Input:</u> a. 0K p(2×2) slab b. 0K c(4×2) slab c. Si bulk (two Si atoms)	1. Surface contributions narrow the bandgap	n/a	n/a	n/a	n/a
Fig 31 (Electronic Density of States)	300K 600K	DFT to calculate Electronic DOS. (averaged over four DOS outputs for the four 600K Si slab snapshots used as input, and averaged over three DOS outputs for the three Si slab 300K snapshots used as input). <u>Input:</u>	• Narrowing bandgap as Temperature increases • Bandgap disappears at a higher Temperature	n/a	n/a	n/a	n/a

Table 4. Summary of results.

<u>Explanatory note for Average Dimer Height</u>

Above = Z difference in dimer height (Z-axis) is positive, i.e., Z>0

Below = Z difference in dimer height (Z-axis) is negative, i.e., Z<0

Dimer 1/ Dimer 2 flip synchronously.

Dimer 3/Dimer 4 flip synchronously.

See the discussion in section 5.1 and 5.1.1 regarding dimer flip synchronization.

6 Conclusion

This MSc project consists of several tasks. It involves, first, a detailed study of the modern concepts in solid state physics and their application to semiconductors, in particular, silicon. These concepts are described, for instance, in the fundamental monographs [34] and [53]. However, a wider choice of the monographs has been considered during the study.

Next, a lot of attention has been devoted to study of the Density Functional Theory (DFT) based numerical formalisms, in particular Car-Parrinello Molecular Dynamics (CPMD) and Born-Oppenheimer Molecular Dynamics (BOMD) [29] , and their implementation in the Quantum Espresso package [1]. This also included learning the relevant computational physics concepts [54].

After finishing these tasks, our attention shifted towards computer simulations (using the Sharcnet supercomputer facilities) of the structural, dynamical, electronic and optical properties of the clean reconstructed Si(100) surface, which is the main semiconductor surface used in modern microelectronics.

As discussed, the main experimentally observed clean Si(100) surface reconstructions, namely p(2x1), p(2x2) and c(4x2), can be formed by different arrangements of tilted dimers. We have proven, using ab-initio computational formalisms, that the dimers are not only tilted, but their tilt is ordered in an alternating manner along the [011] surface direction, thus forming c(4 × 2) and/or p(2 × 2) reconstructions of Si(100). The potential barrier for dimer flipping (within 0.03 - 0.11 eV [15]), leading to c(4 × 2) and the p(2 × 2) structures switching, becomes comparable with the thermal excitation energy above 200K, and dimer flipping. The dimer flipping and its role were the main components of the research, and we have observed dimer flipping in the simulations at temperatures close to 600K. As the result of such nonzero temperature dynamics, we proved that the time-averaged clean Si(100) structure is seen as an apparent p(2×1) reconstruction as seen during a scanning tunneling experiment [43].

In our numerical approaches we combined next the phonon and optical formalisms ([27] and [38]) to calculate temperature-dependent vibrational spectra of the clean Si(100) reconstructed surface and then the surface temperature dependent reflectance anisotropy (RA).

We demonstrate that the vibrational response of the Si(100) reconstructed surface is substantially modified compared to the bulk phonon spectra. This is explained by the different number of neighboring Si atoms (that is coordination number) in the bulk and at the surface. We also observed appearance of the so-called soft phonon modes, absent in the bulk: extra feature in the calculated phonon response at low frequencies. This feature, observed in our theory, indicates a possibility of surface structural phase transitions, which is well proven experimentally.

For the Si(100) surface this corresponds to c(4×2) ↔ p(2×1) order-disorder transition, which leads to observation of an apparent p(2×1) reconstruction at a temperature above 200K. This has been confirmed by numerous experiments (see, e.g., [43] and refs therein).

We also demonstrated numerically that the higher temperature leads to the red shift in frequencies of the DOS peaks for Si(100) surface. DOS for 0K, 300K and 600K temperatures have been simulated. The effect of the DOS red shift with temperature has been observed for the Si bulk [55]. Although the temperature induced shift at a surface should follow the same mechanism, the results of our calculation for the Si(100) surface still have to be confirmed experimentally.

We calculate next the temperature dependent reflectance anisotropy (RA) of the bulk and surface at a temperature of 0K (as in all the previous theoretical models, see, e.g., [41])

The RA results for the Si(100) reconstructions were in agreement with experimental results [10], [43], including a temperature-induced shift of both surface and bulk optical peak to lower energy and broadening. The position of the main bulk peak for the imaginary part of the dielectric constant is 3.7eV (8.7 × 10^14 Hz) which is in good agreement with the theory of [44].

At the higher temperature of 600K, the surface dimer contribution seen at 1.2eV for the 0K temperature reconstructions is shifted left by 0.2eV. The contribution of the surface dimer to the RA (optical response difference between X and Y direction) at a temperature of 600K is also higher than the reconstructions at 0K, and the peak seen at 3.7eV for the 0K reconstructions, is shifted to 3eV at the temperature of 600K.

The shift in the surface dimer contribution to the RA (optical response difference between the X and Y direction) with the temperature increase has been actually observed experimentally. [28]

For the electronic DOS we demonstrate that the bulk DOS shows a larger bandgap of 0.6eV, there are no contributions from surface states. The DOS for the p(2x2) and c(4x2) reconstructions have very similar bandgaps. 0.3eV and 0.25eV respectively, but reduced in comparison to the bulk, (which has a gap of 0.6eV), this is expected theoretically [47]. At the higher temperature (300K) the bandgap is narrowed compared to the 0K reconstructions. This effect is also expected theoretically. At a temperature of 600K we show that the bandgap has disappeared.

Agreement with experimental results and theory [28] is demonstrated, including a temperature-induced shift of both the surface and bulk optical peaks to a lower energy and broadening, while the temperature-induced effects are more pronounced for the surface atoms than for the Si bulk atoms. This conclusion is even better illustrated when the layer-by-layer formalism uses to

efficiently decouple the bulk and surface contributions to temperature dependent both vibrational and optical responses.

7 Further Investigation

In our research we have demonstrated that the temperature induced dynamical effects on the surface phonons, and reconstruction dependent optical response, can be successfully accessed through the combination of ab Initio Molecular dynamics and numerical optical formalisms. Even though the simulations, which were carried out, are demanding computationally, they can be further extended not only for the Si surfaces in a wider range of temperatures, but also for other technologically important semiconductors.

We list below several possible extension of the results, described above.

Item	**Description**
Try to observe numerically Si(100) dimer flipping at room and higher temperatures.	Complete a long CPMD run at 300K and higher temperatures (e.g., 400K and 500K) to see if dimer flipping can be observed at room temperature and above.
Detailed analysis of the top layers atomic motion, especially during dimer flipping to better understand the dimer contribution to the phonon spectra.	Using the dynamical results of various CPMD runs where dimer flipping has occurred, analyze the motion of the atoms in the layers close to the surface to find any interesting behaviors or patterns.
Analysis of anharmonic contribution to the vibrational spectra, which originate from deeper atomic Si layers than the surface.	Use the Velocity Auto Correlation Technique on CPMD dynamics output to look at underlying Si surface layers.
Reaching better defined understanding of the dynamic dimers symmetrization observed for the CPMD 600K run.	Complete a longer BOMD run at 600K to observe dynamical dimer symmetrization.
Analysis of dimer stability and the effect of surface melting.	Complete CPMD and BOMD runs at higher (800K, 1000K and 1200K) temperatures.

8 References

[1] P. Giannozzi, O. Andreussi, T. Brumme, O. Bunau, M. B. Nardelli, M. Calandra, R. Car, C. Cavazzoni, D. Ceresoli, M. Cococcioni*, et al*, Journal of Physics: Condensed Matter **29**, 465901 (2017).
[2] C. Battaglia, K. Gaál-Nagy, C. Monney, C. Didiot, E. F. Schwier, M. G. Garnier, G. Onida, and P. Aebi, Journal of Physics: Condensed Matter **21**, 013001 (2009).
[3] R. E. Camacho-Aguilera, Y. Cai, N. Patel, J. T. Bessette, M. Romagnoli, L. C. Kimerling, and J. Michel, Opt.Express **20**, 11316 (2012).
[4] J. R. Power, P. Weightman, S. Bose, A. I. Shkrebtii, and R. Del Sole, Phys. Rev. Lett. **80**, 3133 (1998).
[5] J. Rathel, E. Speiser, N. Esser, U. Bass, S. Meyer, J. Schäfer, and J. Geurts, Phys.Rev.B **86**, 035312 (2012).
[6] T. Uda, H. Shigekawa, Y. Sugawara, S. Mizuno, H. Tochihara, Y. Yamashita, J. Yoshinobu, K. Nakatsuji, H. Kawai, and F. Komori, Prog Surf Sci **76**, 147 (2004).
[7] A. Selloni, A. Fasolino, and A. I. Shkrebtii, *Landolt-Börnstein: Numerical Data and Functional Relationships in Science and Technology - New Series, Subseries: Condensed Matter 1993 "Surface reconstruction and relaxation"* (Springer-Verlag, Berlin, 1993), Subvolume 24a, p. 125.
[8] D. Haneman, Reports on Progress in Physics **50**, 1045 (1987).
[9] F. Bechstedt, *Principles of Surface Physics* (Springer-Verlag, Berlin, 2003).
[10] A. I. Shkrebtii, R. Di Felice, C. M. Bertoni, and R. Del Sole, Phys.Rev.B **51**, 11201 (1995).
[11] E. Fontes, J. R. Patel, and F. Comin, Phys. Rev. Lett. **70**, 2790 (1993).
[12] A. I. Shkrebtii and R. Del Sole, Phys. Rev. Lett. **70**, 2645 (1993).
[13] E. Landemark, C. J. Karlsson, Y. C. Chao, and R. I. G. Uhrberg, Phys. Rev. Lett. **69**, 1588 (1992).
[14] H. Over, J. Wasserfall, W. Ranke, C. Ambiatello, R. Sawitzki, D. Wolf, and W. Moritz, Phys.Rev.B **55**, 4731 (1997).
[15] K. Hata, Y. Sainoo, and H. Shigekawa, Phys. Rev. Lett. **86**, 3084 (2001).
[16] R. A. Wolkow, Phys. Rev. Lett. **68**, 2636 (1992).
[17] J. Nakamura and A. Natori, Phys.Rev.B **71**, 113303 (2005).
[18] K. Sagisaka, D. Fujita, and G. Kido, Phys. Rev. Lett. **91**, 146103 (2003).
[19] R. Tromp, R. Hamers, and J. Demuth, Phys. Rev. Lett. **55**, 1303 (1985).
[20] H. Neddermeyer, Reports on Progress in Physics **59**, 701 (1996).
[21] R. Felici, I. K. Robinson, C. Ottaviani, P. Imperatori, P. Eng, and P. Perfetti, Surf. Sci. **375**, 55 (1997).
[22] N. D. Kim, Y. K. Kim, C. -. Park, H. W. Yeom, H. Koh, E. Rotenberg, and J. R. Ahn, Phys.Rev.B **75**, 125309 (2007).
[23] T. Yokoyama and K. Takayanagi, Phys.Rev.B **61**, R5078 (2000).
[24] L. Caramella, C. Hogan, G. Onida, and R. Del Sole, Phys.Rev.B **79**, 155447 (2009).
[25] J. Fritsch and P. Pavone, Surf Sci **344**, 159 (1995).
[26] M. Eremtchenko, F. S. Tautz, R. Öttking, and J. A. Schaefer, Surf Sci **600**, 3446 (2006).
[27] S. Baroni, S. de Gironcoli, A. Dal Corso, and P. Giannozzi, Rev. Mod. Phys. **73**, 515 (2001).
[28] A. Shkrebtii and M. Rohlfing, *Part II. "Theoretical Foundations and Simulation of Surface Structures", in "Physics of Solid Surfaces Subvolume B"* (Springer-Verlag GmbH;, 2017), p. 19.
[29] J. Kohanoff, *Electronic Structure Calculations for Solids and Molecules: Theory and Computational Methods* (Cambridge: Cambridge University Press, 2006).
[30] A. Ramstad, G. Brocks, and P. J. Kelly, Phys.Rev.B **51**, 14504 (1995).
[31] P. Hohenberg and W. Kohn, Phys.Rev. **136**, B864 (1964).
[32] W. Kohn and L. J. Sham, Phys.Rev. **140**, A1133 (1965).
[33] D. M. Ceperley and B. J. Alder, Phys.Rev.Lett. **45**, 566 (1980).
[34] C. Kittel, *Introduction to Solid State Physics* (John Wiley and sons, New-York, 2005).

[35] H. J. Monkhorst and J. D. Pack, Phys.Rev.B **13**, 5188 (1976).
[36] P. Giannozzi, S. de Gironcoli, P. Pavone, and S. Baroni, Phys.Rev.B **43**, 7231 (1991).
[37] Z. A. Ibrahim, A. I. Shkrebtii, M. Lee, V. Vynck, T. Teatro, W. Richter, T. Trepk, and T. Zettler, http://arxiv. org/abs/0710. 1020 **Oct.** (2007).
[38] Z. A. Ibrahim, A. I. Shkrebtii, M. Lee, V. Vynck, T. Teatro, W. Richter, T. Trepk, and T. Zettler, Phys. Rev. B **77**, 125218 (2008).
[39] R. E. Schlier and H. E. Farnsworth, J. Chem. Phys. **30**, 917 (1959).
[40] H. Ibach, *Physics of Surfaces and Interfaces* (Springer, 2006).
[41] M. Palummo, N. Witkowski, O. Pluchery, R. Del Sole, and Y. Borensztein, Phys.Rev.B **79**, 035327 (2009).
[42] Z. A. Ibrahim, A. I. Shkrebtii, M. J. G. Lee, T. Teatro, M. Drago, T. Trepk, and W. Richter, in *PHYSICS OF SEMICONDUCTORS: 29th International Conference on the Physics of Semiconductors, Rio de Janeiro (Brazil), Jul 27 - Aug 1, 2008*, edited by M. Caldas and N. Studart (AIP, 2010), p. 61.
[43] M. Dubois, L. Perdigão, C. Delerue, G. Allan, B. Grandidier, D. Deresmes, and D. Stiévenard, Phys.Rev.B **71**, 165322 (2005).
[44] C. Guo, K. Hermann, and Y. Zhao, The Journal of Physical Chemistry C **118**, 25614 (2014).
[45] L. Gavioli, M. G. Betti, C. Mariani, A. I. Shkrebtii, R. Del Sole, C. Cepek, A. Goldoni, and S. Modesti, Surf. Sci. **377-379**, 360 (1997).
[46] Y. Fukaya and Y. Shigeta, Phys. Rev. Lett. **91**, 126103 (2003).
[47] W. Stigler, P. Pavone, U. Schröder, J. Fritsch, G. Brusdeylins, T. Wach, and J. P. Toennies, Phys. Rev. Lett. **79**, 1090 (1997).
[48] I. M. Kupchak, F. Gaspari, A. I. Shkrebtii, and J. M. Perz, J. Appl. Phys. **103**, 123525-1 (2008).
[49] C. A. Meli and E. F. Greene, J. Chem. Phys. **101**, 7139 (1994).
[50] S. G. Jaloviar, J. Lin, F. Liu, V. Zielasek, L. McCaughan, and M. G. Lagally, Phys. Rev. Lett. **82**, 791 (1999).
[51] D. E. Aspnes and A. A. Studna, Phys. Rev. B **27**, 985 (1983).
[52] I. Tamm, Phys. Z. Sowjetunion. **1**, 733 (1932).[53] N. W. Ashcroft and N. D. Mermin, *Solid State Physics* (Thomson Brook/Cole, 1976), p. 826.
[54] T. Pang, *An Introduction to Computational Physics* (Cambridge University Press, 2006).
[55] P. B. Allen and M. Cardona, Phys. Rev. B **27**, 4760 (1983).
[56] Y. Borensztein, (Private communication).
[57] X. Gonze, Phys. Rev. A **52**, 1086 (1995); X. Gonze, Phys. Rev. A **52**, 1096 (1995)
[58] R. N. Barnett and U. Landman, Phys.Rev.B **48**, 2081 (1993).
[59] D.-S.Lin, J.-L. Wu, S.-Y Pan, and T.-C Chiang, Volume 90, Number 4, Physical Review Letters (2003)
[60] Xiao Deng, Pradeep Namboodiri, Kai Li, Xiqiao Wang, Gheorghe Stan, Alline F. Myers, Xinbin Cheng, Tongbao Li, Richard M.Silver, Applied Surface Science (Elsevier), 2016
[61] https://www.tcd.ie/Physics/people/Charles.Patterson/Papers/paper1.pdf
[62] Felicianl Giustino, *Materials Modelling using Density Functional Theory*,, (Oxford University Press, 2014)